LUND UNIVERSITY

Numerical simulation of multi-scale transport processes and reactions in pem fuel cells using two-phase models

Khan, Munir; Yuan, Jinliang; Sundén, Bengt

2009

[Link to publication](#)

Total number of authors:
3

Numerical Simulation of Multi-scale Transport Processes and Reactions in PEM Fuel Cells using Two-Phase Models

Munir Ahmed Khan

Thesis for the degree of Licentiate of Engineering, 2009

Division of Heat Transfer
Department of Energy Sciences
Faculty of Engineering (LTH)
Lund University

www.energy.lth.se

Abstract

A numerical study for the cathode of a PEM fuel cell has been performed in this study. The results have been limited to cathode only because, in PEM fuel cells, the oxygen reduction reactions, ORRs, are considered the rate limiting reactions and govern the fuel cell performance.

The modeling approach utilized the two-phase models involving water phase change for PEM fuel cells i.e. two-phase current (solid and membrane), two-phase flow (gas and liquid water) and two-phase temperature (fluid and solid). The catalyst layer has been modeled using the microscale agglomerate approach where diffusion of oxygen into the agglomerate structure was used to model the reaction rates.

For comparison of the PEM fuel cell performance, detailed study was performed at load conditions of current densities of 0.22, 0.57 and 0.89 A/cm^2 explicitly. A varying fuel cell performance was observed under different loads. At low current densities, the temperature, electro-osmotic drag, irreversible and losses are quite low but the membrane phase conductivity showed a decreasing pattern along the length of the cathode. At higher current density (0.89 A/cm^2), a sharp decrease in the current was observed due to the mass limitation effects, and due to higher water content, the water flooding effect was observed as more prominent than at lower current densities.

The maximum power density for the present case was observed at 0.55 V. By comparing the results of this study and previous study with single phase flow model, it can be seen that this model is more conservative and captures the mass limitation effects to a great extent and the maximum power density as predicted by the single phase models falls in the mass limitation zone.

Acknowledgments

At first, I would like to express my deep gratitude to my supervisors Prof. Bengt Sundén and Docent Jinliang Yuan for providing me the opportunity to study in the division of Heat Transfer. It is really an honor to study and learn in this noble institute. I would also like to thanks for their commitment and guidance throughout the whole period. My warmest thanks to all the colleagues and friends of Heat Transfer division, particularly Helgi, Henrik, Martin, Nina, Andreas, Wamei, Hedvig, Tareq, Sarah and Asim (the name sequence is based on the room closer to the exit) and all others for their help and support.

At the last, many thanks to my parents and my family, who always support, encourage and pray for my success.

Lots of love to my son Adam (haven't seen him yet).

Table of Contents

Table of Tables and Figures

List of Work Presented

1.   Species and temperature distribution in cathode of PEMFC (Appendix A)
2.   LTNE approach to simulate temperature of cathode in a PEMFC (Appendix B)

Nomenclature

a_{agg}	Effective agglomerate surface area ($m^2 \cdot m^{-3}$)
a_{Pt}^{eff}	Effective catalyst surface area ($m^2 \cdot m^{-3}$)
a_c	Cathodic transfer coefficient
a	Water activity
c_p	Specific heat capacity ($J \cdot kg^{-1} \cdot K^{-1}$)
$C_{O_2}^{ref}$	Reference O_2 concentration ($mol \cdot m^{-3}$)
$D_{i,eff}$	Effective diffusivity of species i ($m^2 \cdot s^{-1}$)
E	Theoretical voltage (V)
F	Faraday's constant
H	Henry's constant ($Pa \cdot m^3 \cdot mol^{-1}$)
h_v	Interstitial heat transfer coefficient ($W \cdot m^{-3} \cdot K^{-1}$)
h_{fg}	Latent heat ($J \cdot kg^{-1}$)
$\vec{J}_i$	Mass Flux of species i ($kg \cdot m^{-2} \cdot s^{-1}$)
i	Current density ($A \cdot m^{-2}$)
i_o	exchange current density ($A \cdot m^{-2}$)
K	Absolute permeability (
k_c	Reaction rate constant (s^{-1})
k_{evp}	Evaporation rate constant ($Pa \cdot s^{-1}$)
k_{con}	Condensation rate constant (s^{-1})
k	Thermal co
M_i	Molecular weight of species ($kg \cdot mol^{-1}$)
m_{Pt}	Platinum loading ($kg \cdot m^{-2}$)
$\dot{m}$	Mass transfer rate ($kg \cdot m^3 \cdot s^{-1}$)
$\hat{N}$	Mass Flux ($kg \cdot m^{-2} \cdot s^{-1}$)
NCO	Nominal cathode overpotential (V)
p	Pressure (Pascals)
$\dot{q}$	Volumetric energy source ($W \cdot m^3$)
r	Radius (m)
S	Volumetric source
s	Water Saturation
$\vec{V}$	Diffusive velocity ($m \cdot s^{-1}$)
V	Voltage obtained (V)
$\vec{v}$	Velocity vector ($m \cdot s^{-1}$)
T	Temperature (K)
t	Catalyst layer thickness (m)
R	Universal gas constant ($J \cdot mol^{-1} \cdot K^{-1}$)
X	Species mass fraction
Y	Species molar fraction
z	Number of electrons consumed per mole of reactant

Greek Letters

α	Net drag coefficient of water molecule per proton
δ_{agg}	Thickness of electrolyte film covering an agglomerate (m)
ε_{agg}	Proportion of electrolyte in agglomerate
ε	Porosity of material

ε_c	Porosity of catalyst layer
Φ_L	Theile's modulus
η_{act}	Local activation overpotential (V)
ρ	Density (kg·m^{-3})
μ	Viscosity (Pa·s)
ϕ	Potential difference (V)
ξ	Reciprocal of permeability (m^{-2})
τ	Turtuosity
σ	Conductivity (S m^{-1}) / Surface tension (N m^{-1})
θ_c	Equilibrium contact angle (degrees)
Ω	Ohm

Subscripts and superscripts

agg	Agglomerate
c	Catalyst layer/Capillary
eff	Effective
e	pore
f	Fluid phase
gm	Gas mixture
i	Species (source)
it	Inter transfer
j	Species (destination)
l	Liquid/interface,
m	Membrane phase
N	Nafion
ORR	Oxygen reduction reaction
Pt	Platinum
s	Solid phase
sat	Saturation
w	Water
wv	Water vapor

1. Introduction

In this chapter a short motivation is presented to pick up this work followed with a brief description of Polymer Electrolyte Membrane Fuel Cells (PEMFCs) and various losses that occur in the operation of PEMFCs. At the end PEMFCs are compared to other popular fuel cells.

1.1 Motivation

With depletion of fossil fuels and ever increasing consumption, an alternate energy source is immanent for the survival of the present industrial and fast paced world. Many alternates have been suggested but few stand the opportunity to take over the conventional and very efficient combustion sources. This opportunity for other energy sources is directly linked to present research society as they stand responsible for making them efficient, stable and low cost. The polymer electrolyte membrane (PEM) fuel cells have also emerged as one of the competitive alternatives but still require extensive and in-depth research for full scale commercialization. The advantage carried by PEM fuel cells is that they are very stable, low operating temperature and highly efficient energy producers.

1.2 Overview of PEMFCs

1.2.1 Basic Principle

In simple words, the fuel cell is a device where hydrogen is 'burnt' or 'consumed' to produce electricity directly through a simple reaction as;

$$2H_2 + O_2 \rightarrow 2H_2O \tag{1}$$

The hydrogen gas is fed at the inlet of an anode where it ionizes, releasing electrons and hydrogen ions (or protons). The electrons produced in these reactions must travel through an external circuit for work load and protons must pass through to the cathode where they recombine in presence of oxygen to produce water.

$$2H_2 \xrightarrow{\;Pt\;} 4H^+ + 4e^- \quad (Anode)$$

$$O_2 + 4e^- + 4H^+ \xrightarrow{\;Pt\;} 2H_2O \quad (Cathode) \tag{2}$$
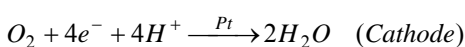
For the operation of PEM fuel cells, some basic essential components are required to carry out the above reactions and serve some of the basic functions as (only few have been stated here);

i)   Feed the hydrogen and Oxygen at anode and cathode, respectively.
ii)   Prevent the direct mixing of the fuels.
iii)   Carry electrical charges through their respective circuits.
iv)   Dissipate energy released during the reactions.
v)   Take out water to prevent flooding etc.
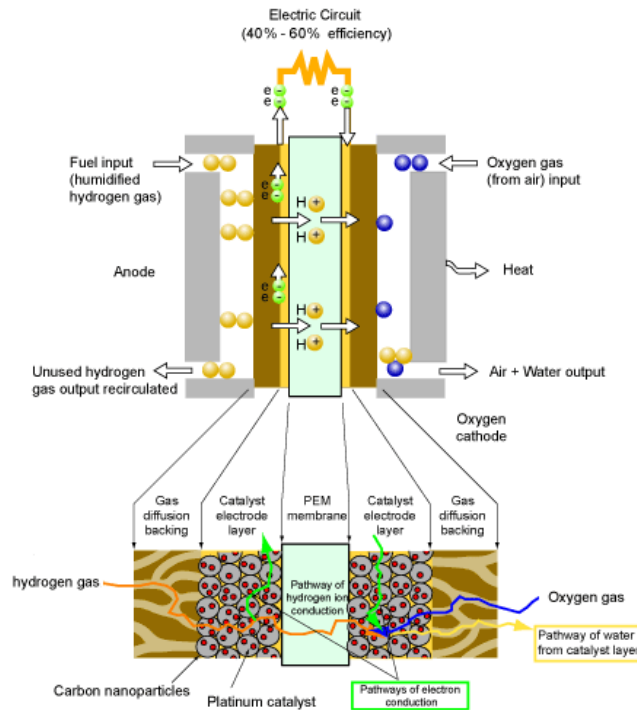
Figure 1: A basic schematic of a PEM fuel cell [1].

So, in order to perform the above functions, some of the basic components essential to ensure safe and efficient operation of the fuel cells are outlined below.

1.2.2 Construction of PEM

In this section only components required for the construction of a single fuel cells will be briefly explained. The discussion about the stacks and accessories for a complete energy unit is out of bound for this work.

The main components of a fuel cell can be outlined as;

i)   Electrolyte
ii)   Catalyst layer (anode and cathode side)
iii)   Gas diffusion layer or porous transport layer
iv)   Bi-polar plates.

Basic schematic of PEM fuel cell is shown in Figure 1 and given below is a brief description of each component.

1.2.2.1 Electrolyte

The electrolyte (or the membrane) constitutes one of the essential components of all types of fuel cells. Mostly, the name given to fuel cells is based on the type of electrolyte used. For PEM fuel cells a polymer membrane is used in between anode and cathode. For PEM fuel cells, the membrane is made by substituting fluorine for hydrogen in long chain polymers and the process is called perfluorination. After this, a side

chain is added, ending with sulphonic acid. The perflourination of the polymer gives it the chemical resistance and mechanical strength while the addition of sulphonic acid gives it the property to carry the positive ions, hydrogen ions in this case. Therefore, the electrolyte in PEM fuel cells is sometimes also called proton exchange membranes. In short all the membranes should essentially have the following properties;

a.   They should be chemically resistant.
b.   They should be strong so that they can be casted in very small thicknesses.
c.   They should be acidic.
d.   They should absorb large quantities of water.
e.   When they are hydrated, hydrogen ion should move freely (higher protonic conductivity).

1.2.2.2 Catalyst Layer

The electrochemical reactions occur in the catalyst layer with the help of Platinum catalyst. Platinum is one the best catalyst for the electrochemical reactions in PEM fuel cells. The basic structure for different designs of PEMs is essentially very similar. The cathode and anode are also of the same design and structure in PEM fuel cells. In the construction, small pt particles are formed on somewhat larger carbon particles. Most often, Cobot is used as carbon particle because of its excellent electrical properties. The platinum is spread out so that high surface area is obtained to the total mass (0.4 to 0.2 mg of Pt/cm^2) [2, 3].

1.2.2.3 Gas Diffusion Layer

The gas diffusion layer (also referred as porous transport layer) essentially serves two very important functions inside PEM fuel cells, given as;

i)   To distribute fuel and oxidant evenly on the catalyst layer.
ii)   Help in effective water removal to avoid water flooding.
iii)   Effectively remove heat generate by electro-chemical reactions.
iv)   Effectively conduct electronic current.

In order to achieve the above results, usually carbon paper or cloth has been selected as GDL. The GDL is also sulphonated to achieve the hydrophobic properties for effective removal of water.

The sandwiched structure of anode side gas diffusion layer and catalyst layer, the membrane and the cathode side catalyst layer and gas diffusion layer is sometimes referred as Membrane Electrode Assembly (MEA), the heart of a single cell. This MEA is placed between the bipolar plates to complete a single of PEM.

1.2.2.4 Bi-Polar Plates

The voltage produced by a single cell is quite small. So, in order to produce usable voltage, many cells have to be connected in series, and, the combination of such cells is called a stack. So, the bi-polar plats serve three functions as;

i)   Connect cells in series
ii)   Collect current
iii)   Provide means of fuel or oxidant distribution evenly in the cell.

For connection and current collection, the bipolar plates are usually made of high electrically conductive material e.g. graphite or stainless steel. For the distribution of fuel and oxidant, these plates have channels cut in them so that gas can flow over the faces of electrodes. At the same time, they are made in such a way that they make a good electrical contact with the surface of each electrode. A three cell stack is shown in Figure 2 using the bi-polar plates
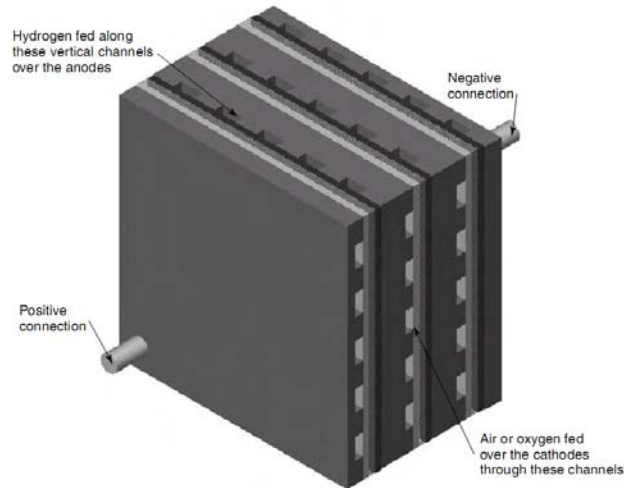
Figure 2: A three cell stack showing the interconnectivity of cells using bi-polar plates [3].

1.2.3 Fuel cell Irreversibilities

It has been a known fact that the actual voltage produced by a fuel cell is always less than the theoretical voltage. The performance of a fuel cell is mostly assessed using the polarization curve that relates the output voltage to the current drawn from a cell. A typical polarization curve for a PEM fuel cell is shown in Figure 3.

Following general features are noticeable in the polarization curve, given as;

    i)   The actual voltage is always less than the theoretical voltage.
    ii)   Initially, there is a sharp decrease in the voltage without any considerable increase in current density.
    iii)   At very high current densities, again, there is sharp decease in the voltage.
    iv)   In-between the decrease is linear.

Such a pattern of the fuel cell behavior can be explained by defining different losses at certain voltages that occur in the fuel cells. The typical losses in a fuel cell are explained below.
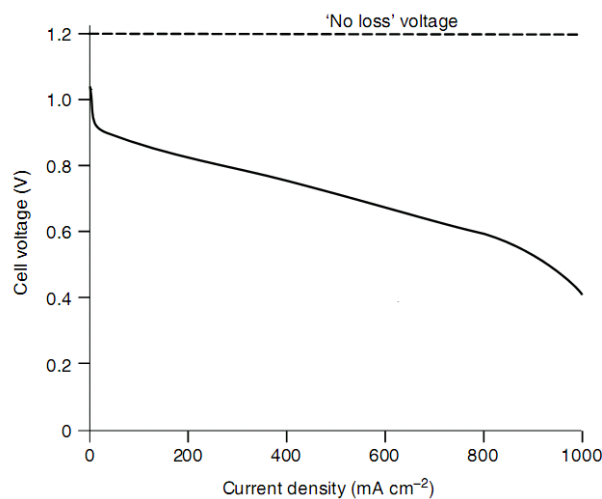
Figure 3: A typical polarization curve for PEM fuel cells.

12

1.2.3.1 Fuel Crossover and internal Currents

The membrane, as discussed, must conduct hydrogen ions, however, there is always fuel diffusion and electron flow through it. This loss in fuel and electrical current is termed as fuel crossover and internal current, respectively.

1.2.3.2 Activation Losses

For every reaction, certain amount of energy barrier has to be crossed to proceed. In fuel cells, electrochemical reactions are accruing at the electrodes. Some of the voltage generated is lost in driving these electro-chemical reactions. This type of loss is highly non linear and results in a sharp decrease at higher voltages.

1.2.3.3 Ohmic Losses

These loses represent the wastage of energy as heat when electrons and protons flow through the respective materials. The ohmic losses are proportional to the voltage and current density, therefore, depicting linear behavior. They are also sometimes referred as resistive losses.

1.2.3.4 Mass Transport Losses

The performance reduction due to the concentration of fuel or oxidant at higher currents are referred as mass transport losses or concentration losses. These losses are considerable at higher currents when the consumption rate is much higher and there is lack of transport of reactants to the reaction site. These type of losses are also highly non linear and can be observed as a sudden drop in voltage at higher current densities.

1.3 Fuel Cell Types and Comparison

Different types of fuel cells have been invented with different operating temperatures, ion carriers and membrane types used for construction. It should be remembered that all fuel cell types are not an alternate to each other but serve as a compliment e.g, PEM fuel cells, inspite of having the highest power density are only limited to kilo Watt range. For higher power extraction i.e. above Mega Watt ranges, the solid oxide fuel cells (SOFCs) are a better option. The types and some of the characteristics of different fuel cells have been presented and compared in Table 1.

Table 1: Some characteristics of important fuel cells[2]						
	PEMFC	**DMFC**	**AFC**	**PAFC**	**MCFC**	**SOFC**
Primary application	Automotive and stationary power	Portable power	Space vehicles and drinking water	Stationary power	Stationary power	Vehicle auxiliary power
Electrolyte	Polymer membrane	Polymer membrane	Concentrated KOH	Concentrated phosphoric acid	Molten carbonate retained in ceramics matrix	Yttrium-stabilized Zirkondioxide
Operating temperature range	50-100°C	0-60°C	50-200°C	150-220°C	600-700°C	700-1000°C
Charge Carrier	H^{+}	H^{+}	OH^{-}	H^{+}	$(CO_3)^{=}$	$O^{=}$

Prime cell components	Carbon based	Carbon based	Carbon based	Graphite based	Stainless steel	Ceramic
Catalyst	Platinum	Pt-Pt/Ru	Platinum	Platinum	Nickel	Perovskites
Primary fuel	H_2	Methanol	H_2	H_2	H_2, CO, CH_4	H_2, CO
Start-up time	Sec – min	Sec – min		Hours	Hours	Hours
Power Density (kW/m^3)	3.8 – 6.5	~0.6	~1	0.8 – 1.9	1.5 – 2.6	0.1 – 1.5
Combined fuel cell efficiency	50 – 60%	30 – 40%	50 – 60%	55%	55 – 65%	55 – 65%

2. Modeling Review

In this chapter a short review will be given about the present and past efforts in the field of PEM fuel cell modeling along with brief history of PEM fuel cells development. Later on problems still faced in PEM modeling will be outlined.

2.1 Historical Background

The first ever PEM fuel cell was developed by General Electric to be used in two-person Gemini Space Vehicle in early 1960s [4]. Instead of proving to be the mile stone in history of PEM fuel cells, this trip to space caused a back lash to the further development of PEM fuel cells. One of the main reasons being the water management inside the cell [3], so, for further space missions Alkaline fuel cells were the preferred choice. In mid 1960s, Dupont developed Nafion membrane that showed improved performance and increased lifetime and, once more, PEM fuel cells were taken to space but this time in biosatellite mission in 1968 [4]. But as before, the water management problem proved to be too difficult to handle. Again, the management and developers of the space program were forced to choose Alkaline fuel cells as an alternate for later missions. In 1970s and early 80s, further development in PEM fuel cells was set aside, mainly due to;

1. PEM fuel cells were more expansive to their counterparts like phosphoric acid (PAFCs) and alkaline fuel cells (AFCs).
2. The membrane and the catalyst (Platinum) were very expensive.
3. PEM fuel cells are very prone to CO poisoning.
4. Water management was too difficult to handle efficiently.

But in late 1980s and early 1990s, the credited efforts of Ballard Power Systems and the Los Alamos National Laboratory, revival of PEM fuel cells occurred by the development of new catalyst loading techniques and membrane properties [5]. And since then, PEM fuel cells have secured a high respect in research industry and many companies are focusing on PEM fuel cells to be used in future products that range from a cell-phone to submarines.

2.2 Classification of Modeling Techniques

On broad sense, the modeling of PEM fuel cells may be classified in different domains based on flow, geometry, catalyst models, phase considered, temperature etc. But all these classifications are only arbitrary because above mentioned parameters are inter-related and no distinct classification line can be drawn.
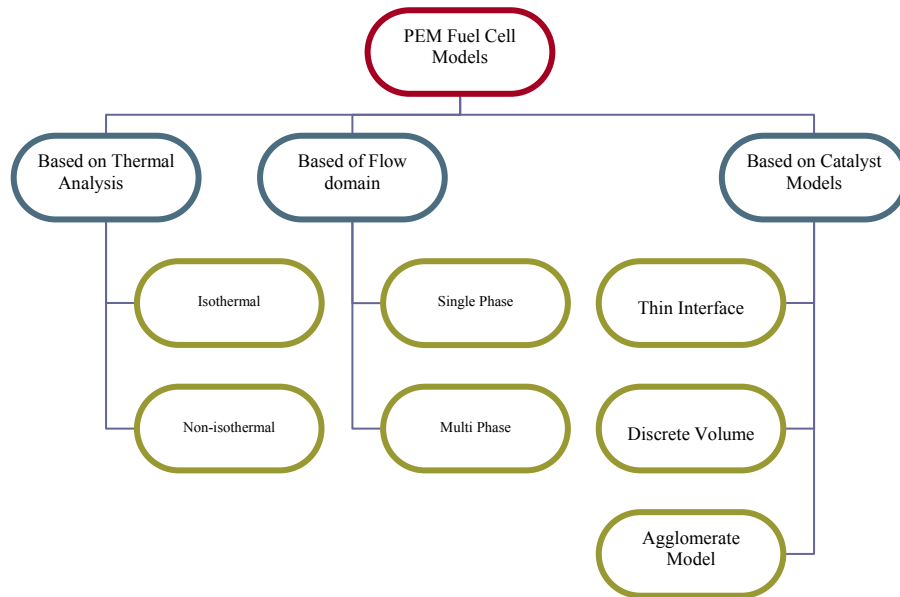
Figure 4: Arbitrary classification of fuel cell models

2.2.1 Models Based on Thermal Analysis

2.2.1.1 Isothermal Models

In isothermal modeling, all the governing equations are solved without considering the temperature effect. Both single- and multi-phase models have been developed in this category with 1-, 2- and 3-D geometries. Many researchers have developed isothermal models that are in good agreement with experimental results. Bernardi [6] developed 1-D model based on basic principles of gas phase transport to find the optimum boundary conditions in order to avoid flooding and dehydration of membrane. Okada et al. [7] later on carried out 1-D theoretical analysis of water transport using a linear transport equation and net drag coefficient to study the effects of inlet humidity on the overall performance of fuel cell. Yi and Nguyen [8] and Wang et al.[9] have also developed 2-D multi-component transport models for a cathode and two-phase flow and reactant transport model, respectively. In the model prescribed by Yi and Nguyen, the inlet air was forced to cross the catalyst layer to study the effects of catalyst layer thickness and Wang et al. reported the dominance of the capillary action in the porous media.

2.2.1.2 Non-Isothermal Models

Regarding the non-isothermal modeling, the effect of heat generation or consumption has to be incorporated as source/sink terms and temperature dependant physical properties of materials. In a fuel cell, heat is generated through different processes e.g. electro-chemical reactions, heat of water vaporization/condensation and heat generated due to charge flow, it is very crucial for complete understanding of the fuel cell processes to include the thermal analysis. Many researchers have worked within this category and produced some effective results as compared to isothermal models. Weber and Newman [10] developed a 1-D non-isothermal model for a single cell in which both heat and mass transfer were coupled together. Their model also accounted for the effects of ohmic losses heat generation due to irreversible reactions. To control the humidification and limit its effects, Nguyen and White [11] developed a 2-D model with various designs. Yuan and Sundén [12] carried out the numerical prediction of heat transfer and gas flow in PEM fuel cell ducts. Effects of thermal conductivity, dimensions of porous media and permeability etc were studied in details. Later on, Yuan et al. [13] performed simulations for two-phase flow and heat transfer in 3-D duct of PEM fuel cells.

2.2.2 Models Based on Flow

2.2.2.1   Single Phase Flow

In a single phase flow, the effect of liquid water present inside the cells is neglected and the humidification of the inflow is limited so that condensation doesn't occur. Garau et al. [14] developed a 1-D model of cathode side of fuel cells and results for various physical and thermodynamic parameters were obtained. Later on, Um et al. [15] carried out 2-D PEM fuel call simulations. This model included electrochemical kinetics, multi-component transport and current distribution. In recent studies, Hwang et al [16, 17] and Sun et al.[18, 19] have composed detail studies regarding the fluid and solid phase temperatures and detailed agglomerate model in single phase flows.

2.2.2.2   Multi-Phase Flow

Since water management is one of the major issues regarding PEM fuel cells, so multi-phase models have better insight into the actual behavior. Different multi-phase models have been developed with different analysis depths. Hwang [20] presented a model of cathode side of PEM with liquid water effects. In his work, the effects of permeability and wetting of porous cathode were studied in depth. Chang et al. [21] also worked with the two-phase flow and developed a transient 1-D model based on agglomerate catalyst structure and investigated the transient transport of gaseous species, protons, and liquid water. Senn and Poulikakos [22] also presented a multi-phase model of diffusion zone in the cathode side of a PEM fuel cell. The effects of downscaling of geometric dimensions on fuel cell performance were studied in their work. Wensheng et al. [23] have also developed a two-phase model of the cathode of PEM fuel cells and investigated the liquid water transport and evaporation, cathode performance under varying cathode pressure and electrode thickness effects on the overall performance of fuel cells. Lately, a two-phase model has been also developed by He et al. [24] in which the droplet size of the liquid water was used to integrate the effects of gas diffusion layer properties and gas drag functions into the effective removal of water from gas channels.

2.2.3 Models Based on Catalyst Layer

Along with the properties of the membrane, the catalyst layer has a very important role in the PEM fuel cells. Since all electro-chemical reactions occur in the catalyst layer, so, an accurate modeling of the catalyst layer is crucial for overall accuracy, reliability and effectiveness of the model. To date, three types of catalyst layer models have been proposed as discussed below;

2.2.3.1   Thin Film Model

In thin film model, the catalyst layer is assumed as an interface between the gas diffusion layer and the membrane comprising of single control volumes [25]. The disadvantage in using thin film model is that it is incapable of capturing the thermal distribution, proton transport, reactant transport and activation over potentials in the catalyst layers [26].

2.2.3.2   Discrete Volume Model

As compared to the thin film models, the discrete volume model is much descriptive in capturing different physical phenomena. This model accounts for heat variation, ohmic losses and overpotentials etc but fails to capture the oxygen dissolution in the electrolyte phase [26] and over-predicts the current density.

2.2.3.3   Agglomerate Model

Among all catalyst layer modeling approaches, the agglomerate model is considered to be most descriptive as it includes the physical aspects of the catalyst layer and captures all regions of the polarization curve in

very effective manner [26]. Even at higher stiochometric ratios, the agglomerate model captures the mass limitations in a well defined manner. Very few attempts have been made to date in applying the agglomerate model to simulate PEM fuel cells. Since, it is very descriptive, it is considered the most expensive in terms of both time and memory for computer resources.

2.3   Present Challenges

Despite the active research in both research organization and industries, only limited commercialization of PEM fuel cells has been observed up till now. Although, many advances have been made in increasing the efficiency, reliability and cost effectiveness but still a few problems are blocking the path to full scale commercialization of PEM fuel cells.

With the advances in the computer technology, the numerical prediction of internal processes has overtaken the experimental study. But since, fuel cells are highly interdisciplinary i.e. they encompass the field of chemistry, materials, thermodynamics and power etc, it is very cumbersome to exactly model real fuel cell behavior under different circumstances. Many researchers have attempted to model the PEM fuel cell behavior, as discussed above, they still lack in completeness. In this work, similar attempt has been made where all three most important phenomena have been considered explicitly for complete understanding of fuel cell response, namely;

i)   Two phase current i.e. solid phase (electric) and membrane phase (protonic).
ii)   Two phase temperature distribution (fluid and solid phase - local thermal non equilibrium approach).
iii)   Two phase flow (gas and liquid) involving water phase change.

For modeling of the catalyst layer, the agglomerate model has been applied to exactly know the reaction response under different conditions.

2.4   Assumptions

Following assumptions have been made for the model presented in this work;

i)   All the processes are time-independent.
ii)   The gas properties are calculated using ideal gas laws.
iii)   The flow is assumed to be laminar in porous media.
iv)   The catalyst layer is composed of spherical agglomerate made of platinum particles supported by carbon and ionomer electrolyte.
v)   The flow of liquid water is independent of gas flow.
vi)   There is no leakage i.e., perfect connection conditions are assumed between all interfaces.
vii)   Local overpotential within an agglomerate is assumed to be constant (verified in [18]).

3.   Mathematical Modeling

In this chapter, the equations implemented for performing the fuel cell simulations have been described. In the present work only the cathode side has been simulated as the oxygen reduction reaction (ORR) is the rate limiting reactions in PEM fuel cells.
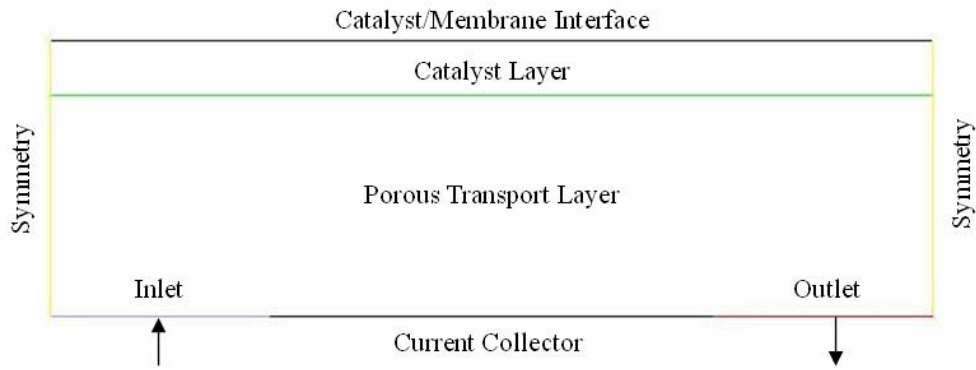
Figure 5: Sketch of cathode of a PEMFC

Figure 5 represents the domain simulated in the present work and the domain dimensions are given in Table 2.

Table 2: Dimensions of cathode for current simulation.

Component	Dimension (mm)
Inlet	0.4
Outlet	0.4
Current Collector	0.8
PTL thickness	0.4
Catalyst layer thickness	0.1

3.1   Continuity and Momentum Equations

The equation for the mass balance, or continuity, can be written as;

$$\nabla \cdot (\rho \vec{v}) = S_m \tag{3}$$

Equation (3) is the general form of the mass conservation equation where S_m represents the source or sink terms for the species. Whereas, the momentum equation can be given as;

$$\nabla \cdot (\rho \vec{v} \vec{v}) = -\nabla p + \nabla \cdot \left(\overline{\overline{\tau}}\right) + \rho \vec{g} + \vec{F} \tag{4}$$

Where p is the static pressure, $\vec{F}$ is the external body force, which in this case comprises of two terms i.e. porous media formulation (explained below) and the source terms due to consumption/production of different species.

$\overline{\overline{\tau}}$ is called the stress tensor and is given by;

$$\overline{\overline{\tau}} = \mu(\nabla \vec{v}) \tag{5}$$

3.2   Porous Media Formulation

Porous media are modeled by an addition of a source term to the momentum equation and using the superficial velocity for all equations. The superficial velocity is given as;

$$\vec{v}_{Darcy} = \varepsilon \vec{v}_{Physical} \tag{6}$$

Where ε is the porosity of the material. The source term for the momentum equation comprises two terms, the viscous loss term (Darcy) and the inertial loss term. In the present scenario, the inertial loss term has been neglected, so, only the Darcy pressure drop has been modeled considering the fact that in laminar flows, the pressure drop is directly proportional to the velocity of flow and is given as;

$$S_i = -\left(\sum_{i=1}^{2} \xi_{ij} \mu v_j\right) \tag{7}$$

Where ξ_{ij} is the reciprocal of the permeability of the porous media.

3.3   Multiphase Flow

As already mentioned earlier, the PEM fuel cells fall into two phase flow domain including gas phase (air and water vapor) and liquid water. In the present model, the transport process of both gas and liquid, separate equations have been applied as described below;

3.3.1 Gas Phase Transport

The gas transport has been simulated by using the species equation as;

$$\nabla \cdot (\rho \vec{v} X_i) = -\nabla \cdot \vec{J}_i + R_i + S_i \tag{8}$$

Equation (8) represents the transport equation for the cathode species in terms of mass fractions. R_i is the rate of production of species i due to the chemical reaction while S_i accumulates all other sources due to evaporation/condensation processes.

$\vec{J}_i$ is the mass flux arising due to the species concentration gradients in the flow field. A careful treatment of species diffusion transport is very essential in diffusion – dominated laminar flows. Here, the Maxwell – Stefan equations have been used to obtain the diffusive mass flux.

The Maxwell-Stefan equation can be written as [27];

$$\sum_{\substack{j=1 \\ j \neq i}}^{N} \frac{Y_i Y_j}{D_{i,j}} \left(\vec{V}_j - \vec{V}_i \right) = \vec{d}_i - \frac{\nabla T}{T} \sum_{\substack{j=1 \\ j \neq i}}^{N} \frac{Y_i Y_j}{D_{i,j}} \left(\frac{D_{T,j}}{\rho_j} - \frac{D_{T,j}}{\rho_i} \right) \tag{9}$$

Where Y is the mole fraction, $\vec{V}$ is the diffusion velocity, $D_{i,j}$ is the binary mass diffusion coefficient and D_T is the thermal diffusion coefficient. Since, the temperature gradients in PEM fuel cells are not high, the thermal diffusion effect can be safely neglected. So, $D_T = 0$ has been assumed in this case, reducing the equation to;

$$\sum_{\substack{j=1 \\ j \neq i}}^{N} \frac{Y_i Y_j}{D_{i,j}} \left(\vec{V}_j - \vec{V}_i \right) = \vec{d}_i \tag{10}$$

For an ideal gas the Maxwell diffusion coefficient are equal to binary diffusion coefficients. Neglecting pressure diffusion and assuming equal force on all species, then; $\vec{d}_i = \nabla Y_i$ and $\vec{J}_i = \rho_i \vec{V}_i$., and substitution in Equation (10) yields;

$$\sum_{\substack{j=1 \\ j \neq i}}^{N} \frac{Y_i Y_j}{D_{i,j}} \left(\frac{\vec{J}_j}{\rho_j} - \frac{\vec{J}_i}{\rho_i} \right) = \nabla Y_i \tag{11}$$

and, after some mathematical manipulation, the diffusive mass flux vector can be obtained from [28];

$$\vec{J}_i = -\sum_{j=1}^{N-1} \rho D_{ij} \nabla X_i \tag{12}$$

The binary diffusion coefficient can be calculated as;

$$D_{ij} = [D] = [A]^{-1} [B] \tag{13}$$

$$A_{ii} = -\left(\frac{Y_i}{D_{iN}} \frac{M_w}{M_{w,N}} + \sum_{\substack{j=1 \\ j \neq 1}}^{N} \frac{Y_i}{D_{ij}} \frac{M_w}{M_{w,i}} \right) \tag{14}$$

$$A_{ij} = Y_i \left(\frac{1}{D_{ij}} \frac{M_w}{M_{w,j}} - \frac{1}{D_{iN}} \frac{M_w}{M_{w,N}} \right) \tag{15}$$

$$B_{ii} = -\left(Y_i \frac{M_w}{M_{w,N}} + \left(1 - Y_i \right) \frac{M_w}{M_{w,i}} \right) \tag{16}$$

$$B_{ij} = Y_i \left(\frac{M_w}{M_{w,j}} - \frac{M_w}{M_{w,N}} \right) \tag{17}$$

Since the catalyst layer and the PTL are both porous media, Knudsen diffusion is an active phenomenon and needs to be also accounted in the model [29].

$$D_{i,k} = \frac{2}{3} r_e v_i = \frac{2}{3} r_e \sqrt{\left(\frac{8RT}{\pi M_i}\right)} \tag{18}$$

In the present model an effective diffusion coefficient has been estimated based on both molecular and Knudsen diffusion given as [30]:

$$D_{i,eff} = \varepsilon^\tau \left(\frac{D_{i,gm} \times D_{i,k}}{D_{i,gm} + D_{i,k}}\right) \tag{19}$$

Where ε^τ is the porosity correction for the porous media.

3.3.2 Liquid Water Transport

As it has been already mentioned in previous chapters that the PEM fuel cells have the advantage of operating at low pressure and temperature. But, this advantage at low current densities may become a severe problem at higher current densities causing flooding of the porous media and hindering the flow of air. For complete picture of PEM fuel cell operations, the effect due to water flooding has to be accounted. In the present work, the liquid water transport has been modeled by using the equation for water saturation (volume fraction of liquid water) given as follows [31, 32];

$$\nabla \cdot \left(\rho_l \vec{V} s\right) = R_w \tag{20}$$

Inside the cathode, it has been assumed that flow of liquid water is governed by the diffusion of liquid water due to capillary pressure, so, the convective term in Equation (20) is replaced by a diffusive term as given below [24];

$$\vec{V} = \frac{K s^3}{\mu_l} \frac{dp_c}{ds} \nabla s \tag{21}$$

Where p_c is the capillary pressure and depends on the hydro-phobic or phallic properties of the materials and is given as [24];

$$p_c = \begin{cases} \dfrac{\sigma \cos\theta_c}{\left(K/\varepsilon\right)^{0.5}} \left(1.417(1-s) - 2.12(1-s)^2 + 1.263(1-s)^3\right) & \theta_c < 90^o \\[4mm] \dfrac{\sigma \cos\theta_c}{\left(K/\varepsilon\right)^{0.5}} \left(1.417s - 2.12s^2 + 1.263s^3\right) & \theta_c > 90^o \end{cases} \tag{22}$$

The term R_w in Equation (20) represents the source term for the evaporation and condensation of the liquid water and water vapor in air, respectively. The amount transfer rate is proportional to the amount of reactant and the difference between water-vapor partial pressure and its saturation pressure, i.e. [20];

$$\dot{m}_{phase} = \begin{cases} k_{con}(1-s)X_{H_2O}\dfrac{P_{H_2O} - P_{H_2O}^{sat}}{RT_f} & if \quad P_{H_2O} - P_{H_2O}^{sat} \geq 0 \\[4mm] k_{evp}s\dfrac{\rho_w}{M_{H_2O}}\left(P_{H_2O} - P_{H_2O}^{sat}\right) & if \quad P_{H_2O} - P_{H_2O}^{sat} < 0 \end{cases} \tag{23}$$

$P_{H_2O}^{sat}$ represents the saturation pressure of air at a local temperature and is correlated using an empirical relation given as [33];

$$\log_{10} P_{H_2O}^{sat} = \begin{pmatrix} -2.1794 + 0.02953(T_f - 273.15) - 9.1837 \\ \times 10^{-5}(T_f - 273.15)^2 + 1.4454 \times 10^{-7}(T_f - 273.15)^3 \end{pmatrix} \tag{24}$$

The effect of liquid water is incorporated into simulation by multiplying the value of water saturation *s* to the porosity (Equation (6) and the reaction rate equations described later in this chapter).

Along side evaporation and condensation processes, there is also a movement of water between anode and cathode due to;

    1.   Electro-osmotic drag due to charge transport
    2.   Back-diffusion due to concentration gradient of water
    3.   convection due to pressure gradients (neglected in this work)

The electro-osmotic drag and back-diffusion can be interconnected using the net drag coefficient of water [26, 34-36] as a source term for Equation (20).

$$\alpha_{H_2O} = \begin{cases} 1.0 & if \quad NCO < 0.25\,V \\ 46 \times NCO^2 - 31.52 \times NCO + 5.7 & if \quad 0.25 \geq NCO \leq 0.35\,V \\ 0.3 & if \quad NCO > 0.35\,V \end{cases} \tag{25}$$

The correlation in Equation (25) has been formulated in [37] and further modified to involve current density and cathode potential, NCO, in [18].

3.4 Temperature Distribution

Since electrochemical reactions are accruing in the catalyst layer of a fuel cell, and the reactions being exothermic in nature, supply heat energy to both fluid (gas and liquid) and the solid phases. In the present simulation a two phase temperature approach [17, 20, 38] has been applied.

3.4.1 Fluid Phase Temperature

The general energy equation for the fluid phase is given as;

$$\nabla \cdot (\rho c_p T_f) = \nabla \cdot (k_{eff} \nabla T_f) + S_f \tag{26}$$

where k_{eff} is the effective thermal conductivity of the fluid phase. The source term S_f in Equation (26) includes all the external sinks and sources of heat e.g. heat due to chemical reactions, mass transfer, ohmic losses and the energy transfer due to the phase temperature difference of fluid and solid phase. The values for all sources are given in Table 3.

For the gas diffusion layer the source term in Equation (26) is given as:

$$S_f = -\dot{q}_{it} + \dot{q}_{phase} \tag{27}$$

In Equation (27)27, the source term $\dot{q}_{it}$ stands for the intrinsic heat transfer between the solid matrix and the reactant fluids, and the phase change heat transfer, $\dot{q}_{phase}$, which is given as the product of the latent heat of evaporation/condensation and the interfacial mass transfer rate as determined by Equation (23), i.e.;

$$\dot{q}_{phase} = \left\{ \begin{array}{ll} k_{con}(1-s)X_{H_2O} \dfrac{P_{H_2O} - P_{H_2O}^{sat}}{RT_f} & if \quad P_{H_2O} - P_{H_2O}^{sat} \geq 0 \\[4mm] k_{evp} s \dfrac{\rho_w}{M_{H_2O}} \left(P_{H_2O} - P_{H_2O}^{sat} \right) & if \quad P_{H_2O} - P_{H_2O}^{sat} < 0 \end{array} \right\} \times h_{fg} \tag{28}$$

The quantity $\dot{q}_{phase}$ is strongly dependant on the fluid temperature. First, the latent heat of phase change is a function of the fluid temperature and secondly, if condensation occurs, the quantity $\dot{m}_{Phase}$ will be positive; thus $\dot{q}_{phase} > 0$, i.e., the condensation will heat up the control volume. An increase in the fluid phase temperature will increase the saturation pressure of water vapors. Thus, driving force for condensation $\left(P_{H_2O} - P_{H_2O}^{sat} \right)$ will decrease, resulting in an increase in the condensation rate.

For the catalyst layer, the source term in Equation (26) is given as;

$$S_f = \dot{q}_{ORR} + \dot{q}_\Omega + \dot{q}_{phase} \tag{29}$$

where the term $\dot{q}_{ORR}$ represents the heating due to the oxygen reduction reactions occurring at the catalyst layer of the cathode as given in **Error! Reference source not found.**

3.4.2 Solid Phase Temperature

The solid phase (matrix) of the cathode is modeled by using the diffusive temperature equation in the GDL where thermal non-equilibrium approach has been utilized [16, 17, 20, 38, 39]. The energy equation of the solid phase is given as:

$$0 = \nabla \cdot \left(k_{eff} \nabla T_f \right) + S_s \tag{30}$$

In the catalyst layer, using the fact that the reactions are accuring at the interface of solid and fluid materials, both are assumed at the thermal equilibrium [16, 17, 20, 38, 39] i.e.:

$$T_{f,catalyst} = T_{s,catalyst} \tag{31}$$

The source term S_s in Equation (30) for GDL is given as;

$$S_s = -\dot{q}_{it} + \dot{q}_\Omega \tag{32}$$

3.5 Charge Transport

In the PEM fuel cells, there are two types of current flowing through the domain, i.e.;

1   Flow of electrons through the external circuit and the solid matrix, so, called the solid phase current, and,

2   Flow of Hydrogen ions (protons) through the membrane from anode to cathode called membrane phase current.

Table 3: Source terms in two phase models

Equations	Source term	Gas Diffusion Layer (GDL)	Catalyst Layer (CL)
Momentum	$\dot{m}_{ORR,O_2}$	0	$-\dfrac{M_{O_2}}{4F}\nabla\cdot i$
	$\dot{m}_{ORR,H_2O}$	0	$\dfrac{M_{H_2O}}{2F}\nabla\cdot i$
	$\dot{m}_{Phase}$	Equation (23)	Equation (23)
Energy	$\dot{q}_\Omega$	$\dfrac{i_s^2}{\sigma_{s,eff}}$	$\dfrac{i_s^2}{\sigma_{s,eff}}+\dfrac{i_m^2}{\sigma_{m,eff}}$
	$\dot{q}_{phase}$	$\dot{m}_{phase}\times h_{fg}$	$\dot{m}_{phase}\times h_{fg}$
	$\dot{q}_{it}$	$h_v\left(T_s-T_f\right)$	0
	$\dot{q}_{ORR}$	0	$\left(\phi_m-\phi_s\right)\times\nabla\cdot i$
Charge	S_{ϕ_s}	0	$\nabla\cdot i$
	S_{ϕ_m}	0	$-\nabla\cdot i$

3.5.1 Solid Phase Current

Electrons in the catalyst layer are transported through the solid matrix by conduction due to the solid phase potential difference between the catalyst layer and the current collector. The governing equation for the modeling of solid phase potential is given as [18, 26, 40]:

$$-\nabla\cdot\left(\sigma_s\nabla\phi_s\right)=S_{\phi_s} \tag{33}$$

Where S_{ϕ_s} is the source term for the solid phase current equation per unit volume and applicable to the catalyst layer only as given in **Error! Reference source not found.**. The solid conductivity σ_s of the solid phase current is the function of both the volume percent of solid portion in the domain and the electrolyte and reads as;

$$\sigma_s=\sigma_o\left[\left(1-\varepsilon\right)\left(1-\phi_{agg}\right)\right]^{1.5} \tag{34}$$

The term ϕ_{agg} represents the fraction of electrolyte (conducting material) in the domain for the charge transfer.

3.5.2 Membrane Phase Current

The flow of hydrogen ions (protons) from anode to cathode through the membrane comprise the membrane phase current where the hydrogen ions are consumed at the catalyst layer of cathode to form water. The driving force for the protons is called the membrane phase potential and is modeled as:

$$-\nabla\cdot\left(\sigma_m\nabla\phi_m\right)=S_{\phi_m} \tag{35}$$

The source term for Equation (35) is given in Table 3. The conductivity for the protonic current is a function of the water content in the domain and is reads as [41];

$$\sigma_m = \beta(0.514\lambda - 0.326)^{\varpi} e^{1268\left(\frac{1}{303} - \frac{1}{T_f}\right)}$$ (36)

The water content, λ, in Equation (36), is correlated as [42];

$$\lambda = \begin{cases} 0.043 + 17.18a - 39.85a^2 + 36a^3 & if \quad a > 1 \\ 14 + 1.4(a-1) & if \quad a < 1 \end{cases}$$ (37)

Where a is the water activity and is represented in terms of total water present both in vapor and liquid phases.

$$a = \frac{P_{wv}}{P_{sat}} + 2s$$ (38)

3.5.3 Activation Overpotential and Cathode Potential

Some of the energy is consumed for driving the electrochemical reaction [3]. The energy required to carry out the reactions can be estimated as [18, 19]:

$$\eta_{act} = \phi_{s,l} - \phi_{m,l} - \phi_{ref}$$ (39)

Where $\phi_{s,l}$ and $\phi_{m,l}$ are the local solid phase and membrane phase potentials, respectively. ϕ_{ref} is the reference potential and depends on the type of electrode. Since, in this work, only the cathode side has been modeled, so, the reference potential is set to zero [18, 19, 26]. The difference in the membrane phase potential at catalyst/membrane interface and solid phase potential at the current collector is called the nominal cathode overpotential (*NCO*). The advantage for using the *NCO* is that it is descriptive of total losses in the cathode i.e. activation, ohmic and mass transport losses. The overall voltage of the cathode is related to *NCO* by [26]:

$$V_{cathode} = E_{theoratical} - NCO$$ (40)

where $E_{theoratical}$ is calculated as [13]:

$$E_{theoratical} = 1.229 - 0.85 \times 10^{-3} T + 4.31 \times 10^{-5} T \left[\ln(P_{H_2}) + \frac{1}{2}\ln(P_{O_2}) \right]$$ (41)

3.6 Microscopic Reactions Model for Catalyst Layer

In the present work, the agglomerate model has been applied for the modeling for determination of reaction rate as it is the most descriptive of all and accounts for more physical processes including the actual morphology of the catalyst layer as compared to other catalyst layer models [26].

The agglomerate model presented in this work is based on the following assumptions:

1. The catalyst layer is composed of agglomerates made of mixture of platinum supported on carbon and ionomer electrolyte, and is surrounded by voids.
2. The electrochemical reactions occur inside the agglomerate.
3. The reactant species reach the reaction side by both convection and diffusion first and then dissolves through the electrolyte engulfing the agglomerate.
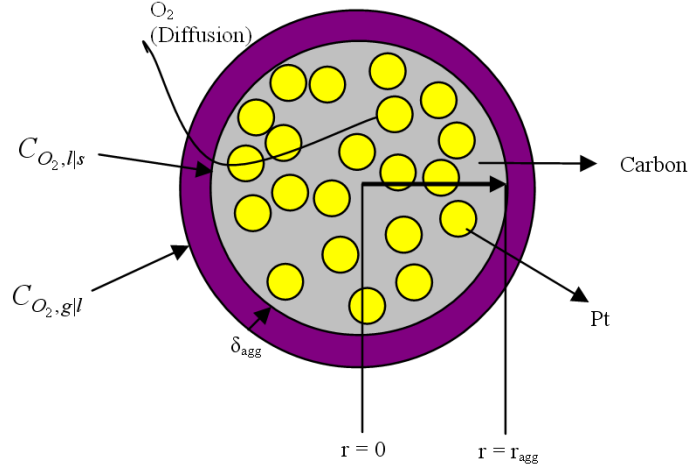
Figure 6: Agglomerate and electrolyte covering of an agglomerate [18, 40]

In the agglomerate model, when oxygen reaches the agglomerate surface, it dissolves into the electrolyte and diffuses through the electrolyte film surrounding the agglomerate as depicted in Figure 5. The transport process can be described as [18, 40];

$$\hat{N}_{O_2} = D_{O_2,E} \frac{\partial C_{O_2}}{\partial r} = D_{O_2,N} \frac{r_{agg}}{r_{agg} + \delta_{agg}} \frac{C_{O_2,g|l} - C_{O_2,l|s}}{\delta_{agg}}$$ (42)

Where $\hat{N}_{O_2}$ is the oxygen flux through the agglomerate boundary, $C_{O_2,g|l}$ is the concentration of dissolved oxygen inside the agglomerate and $C_{O_2,g|s}$ is the oxygen gas concentration at the agglomerate surface. $D_{O_2,N}$ represents the oxygen gas diffusion coefficient through the Nafion thickness. Diffusion process can be related to the reaction rate as [18, 40];

$$D^{eff} \frac{1}{r^2} \frac{\partial}{\partial r} \left(r^2 \frac{\partial}{\partial r} C_{O_2} \right) = -C_{O_2} k_c$$ (43)

k_c is the reaction rate and D^{eff} is the Bruggemann corrected diffusivity of oxygen inside agglomerate and is given as;

$$D^{eff} = D_{O_2,N} \varepsilon_{agg}^{1.5}$$ (44)

The mass balance for the oxygen in the catalyst layer, based on above description, is given as [18, 40];

$$\nabla \cdot N_{O_2} + a_{agg} \hat{N} = 0$$ (45)

$$\nabla \cdot N_{O_2} + R_{O_2} = 0$$ (46)

3.6.1 Oxygen Reduction in Agglomerate

The overall oxygen reduction reaction (ORR) mechanism at the cathode has not been fully explored but it is observed that the ORR follows first order kinetics with respect to oxygen concentration [18, 43];

$$R_{ORR} = k_c C_{O_2} \tag{47}$$

Where k_c is the reaction rate constant. The consumption of oxygen in the electrochemical reactions in the agglomerate can be expressed in terms of the concentration of oxygen at the outer surface of the agglomerate i.e.;

$$R_{ORR} = E_{ORR} k_c C_{O_2 l|s} \tag{48}$$

where E_{ORR} is the effectiveness of the agglomerate reactions for spherical geometries. The effectiveness factor for the spherical agglomerate structure is given as [18, 19, 26];

$$E_{ORR} = \frac{1}{\phi_L} \left(\frac{1}{\tanh(3\phi_L)} - \frac{1}{3\phi_L} \right) \tag{49}$$

ϕ_L is the non-dimensional Thiele's modulus for chemical reactions and has been correlated as [18, 19, 26];

$$\phi_L = \frac{r_{agg}}{3} \sqrt{\frac{k_c}{D^{eff}}} \tag{50}$$

3.6.2 Electrochemical Reactions

For a control volume, the local current density can be given as [18, 19, 26, 44];

$$\nabla \cdot i = a_{Pt}^{eff} i_o^{reff} \frac{C_{O_2}}{C_{O_2}^{reff}} \left[\exp\left(-\frac{\alpha_c F}{RT} \eta_{act} \right) - \exp\left(\frac{(1-\alpha_c)F}{RT} \eta_{act} \right) \right] \tag{51}$$

In Equation (51), effective platinum surface area a_{Pt}^{eff} approach has been utilized because this approach utilizes the platinum loading effect instead of assuming constant reaction rate throughout the catalyst layer [18, 19, 26, 44]. The effective platinum surface area can be calculated as [40];

$$a_{Pt}^{eff} = \varepsilon_{pt} \frac{m_{Pt}}{t_{cat}} \frac{3}{r_{pt} \rho_{pt}} \tag{52}$$

The oxygen consumption rate can be related to the current density as [18, 19];

$$\nabla \cdot i = -4F\nabla \cdot \left(N_{O_2} \right) \tag{53}$$

or;

$$\nabla \cdot i = 4FR_{O_2} \tag{54}$$

$$\nabla \cdot i = -4FR_{ORR} \left(1 - \varepsilon_c \right) \tag{55}$$

Substituting Equation (48);

$$\nabla \cdot i = 4FE_{ORR} k_c \left(1 - \varepsilon_c \right) C_{O_2, l|s} \tag{56}$$

After detailed rearrangement as performed by [18, 19], the current density divergence can be obtained as:

$$\nabla \cdot i = \frac{4FP_{O_2}}{H\left(\dfrac{1}{E_{ORR}k_c(1-\varepsilon_{cat})} + \dfrac{(r_{agg}+\delta)\delta}{a_{agg}r_{agg}D}\right)}$$

(57)

Where the ratio of oxygen partial pressure to Henry's constant represent the concentration of oxygen at the outer surface of the agglomerate, $C_{O_2,g|l}$.

In order to accommodate the liquid water effect (flooding), the current density divergence is multiplied by $(1-s)$, whereas, as discussed previously, k_c is the reaction rate constant and is evaluated as [18, 19];

$$k_c = \left(\frac{a_{Pt}^{reff}}{4F(1-\varepsilon_{cat})t_{cat}}\right)\left[\frac{i_o^{reff}}{C_{O_2}^{reff}}\right]\left[\exp\left(-\frac{\alpha_c F}{RT}\eta_{act}\right) - \exp\left(\frac{(1-\alpha_c)F}{RT}\eta_{act}\right)\right]$$

(58)

3.6.3 ORR Kinetic Parameters

The exchange current density has been correlated by an Arrhenius-type relationship as [18, 26];

$$\frac{i_{o,2}}{i_{o,1}} = \exp\left[-\frac{\Delta E}{R}\left(\frac{1}{T_2}-\frac{1}{T_1}\right)\right]$$

(59)

The activation energy ΔE has been estimated as 76.5 and 27.7 kJ/mol at low and high slope regions, respectively [18, 26].

3.6.4 Oxygen Gas Diffusion in Nafion

For the present study, Nafion™ has been used as electrolyte. So, the diffusion of oxygen in the electrolyte is given as [21]:

$$D_{O_2,N} = 0.0031 \times 10^{-4} \exp\left(-\frac{2768}{T}\right)$$

(60)

3.6.5 Henry's Constant

Henry's constant determines the variation of oxygen solubility with temperature variation. The correlation used in this work is given as [18, 19, 26];

$$\frac{H_{O_2,1}}{H_{O_2,2}} = \exp\left(-\frac{\Delta G}{R}\left(\frac{1}{T_2}-\frac{1}{T_1}\right)\right)$$

(61)

ΔG, called the free energy of dissolution, is estimated to be 5.21 kJ/mol in [18, 19, 26].

3.7 Numerical Solution

All the simulations have been performed in double precision ANSYS Fluent 12. User Defined Functions (UDFs) were used to implement the flow, geometric and material properties and source terms as given in Table 3. The liquid water, solid and membrane phase potentials were modeled using the User Defined Scalars (UDSs). Initial geometry and grid was developed in Gambit software and then adjusted inside the Fluent software to get satisfactory results.

3.7.1 Solution Methodologies

The coupled scheme has been used for pressure-velocity coupling with 3rd order MUSCL spatial discretization scheme. The residual monitor was limited to 10^{-6} with under-relaxation factors of 0.3, 0.3 and 0.04 for pressure, momentum and water saturation. The grid resolution was adjusted using the grid adoption as shown in Figure 7.
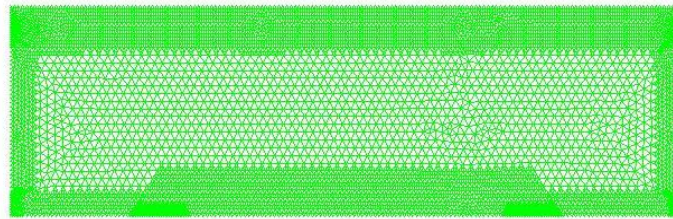
Figure 7: Grid adoption for cathode simulation

The results from adopted grid (11,789 cells) were compared to those with 15,000 and 20,000 cells and it was found that the variation in result for temperature and liquid water was less than 0.01 %, whereas, the simulation time was reduced by 35% and 58% as compared to the simulation time consumed by 15,000 and 20,000 mesh.

Table 4: Operating and design parameters

Parameters	Value	Units	Source(s)
Operating Pressure (absolute)	1.5	atm	
Inlet Temperature	340	K	
Oxygen/Water Vapor ratio	Varied	-	
Porosity of Catalyst Layer	42%	-	[16]
Porosity of Gas Diffusion Layer	48%	-	[16]
Platinum Loading m_{Pt}	0.4	mg·cm^{-2}	[18, 19, 26, 40]
Radius of agglomerate r_{agg}	1	μm	[18, 19, 26, 40]
Specific agglomerate surface area a_{agg}	3.6×10^5	m^2·m^3	[18, 19, 26]
Solid phase conductivity σ_o	100	S·m^{-1}	[18, 19, 26]
Electrolyte film thickness covering agglomerate δ	80	nm	[18, 19, 26]
Electrolyte fraction in agglomerate ε_{agg}	50%	-	
Gas diffusion layer permeability	1.573×10^{-12}	m^2	[16, 17]
Catalyst layer permeability	1.023×10^{-12}	m^2	[16, 17]
Reference O$_2$ concentration $C_{O_2}^{reff}$	0.85	mol·m^{-3}	[18, 19, 26]
Effective Pt surface ratio ε_{Pt}	75%	-	[18, 19, 26]
Henry's constant $H_{O_2,1}$	0.3125	atm·m^2·mol^{-1}	
Heat transfer Coefficient h_v	450×10^6	W·m^{-3}	[20]

Reference exchange current density i_o^{reff}	3.85×10^{-4} (≥ 0.8 V)	A·m^{-2}	[18, 19, 26]
	1.5×10^{-2} (< 0.8 V)	A·m^{-2}	
Cathode transfer coefficient α_c	1 (≥ 0.8 V)	-	[18, 19, 26]
	0.61 (< 0.8 V)	-	

σ

3.7.2 Boundary Conditions

The boundary conditions as implemented during the simulations are given in Table 5.

Table 5: Boundary conditions for the simulation domain

Boundary	Parameter	Value
Inlet	Oxygen mass fraction	0.2284
	Water vapor mass fraction	0.041
	Temperature (Fluid)	$T_{f,in} = 340K$
	Temperature (Solid)	-
	Liquid water	0
	Solid phase potential	$\dfrac{\partial \phi_s}{\partial y} = 0$
	Membrane phase potential	-
Outlet	Oxygen mass fraction	$\dfrac{\partial X_{O_2}}{\partial y} = 0$
	Water vapor mass fraction	$\dfrac{\partial X_{H_2O,wv}}{\partial y} = 0$
	Temperature (Fluid)	$\dfrac{\partial T_{f,out}}{\partial y} = 0$
	Temperature (Solid)	$\dfrac{\partial T_{s,out}}{\partial y} = f(T_f)$
	Liquid water	0
	Solid phase potential	$\dfrac{\partial \phi_s}{\partial y} = 0$
	Membrane phase potential	-
Current Collector	Oxygen mass fraction	$\dfrac{\partial X_{O_2}}{\partial y} = 0$
	Water vapor mass fraction	$\dfrac{\partial X_{H_2O,wv}}{\partial y} = 0$
	Temperature (Fluid)	$\dfrac{\partial T_{f,out}}{\partial y} = f(T_s)$
	Temperature (Solid)	$T_s = 340K$
	Liquid water	$\dfrac{\partial s}{\partial y} = 0$
	Solid phase potential	0
	Membrane phase potential	-

Membrane/Catalyst Interface	Oxygen mass fraction	$\dfrac{\partial X_{O_2}}{\partial y} = 0$
	Water vapor mass fraction	$\dfrac{\partial X_{H_2O,wv}}{\partial y} = 0$
	Temperature (Fluid)	$\dfrac{\partial T_f}{\partial y} = 0$
	Temperature (Solid)	$\dfrac{\partial T_s}{\partial y} = 0$
	Liquid water	$\dfrac{\partial s}{\partial y} = 0$
	Solid phase potential	$\dfrac{\partial \phi_s}{\partial y} = 0$
	Membrane phase potential	$\phi_{mem} = BC$
Symmetric Boundaries	Oxygen mass fraction	$\dfrac{\partial X_{O_2}}{\partial y} = 0$
	Water vapor mass fraction	$\dfrac{\partial X_{H_2O,wv}}{\partial y} = 0$
	Temperature (Fluid)	$\dfrac{\partial T_f}{\partial y} = 0$
	Temperature (Solid)	$\dfrac{\partial T_s}{\partial y} = 0$
	Liquid water	$\dfrac{\partial s}{\partial y} = 0$
	Solid phase potential	$\dfrac{\partial \phi_s}{\partial y} = 0$
	Membrane phase potential	$\dfrac{\partial \phi_{mem}}{\partial y} = 0$
Catalyst/GDL Interface	Membrane phase potential	$\dfrac{\partial \phi_{mem}}{\partial y} = 0$

4. Results and Discussion

In this chapter, the results obtained are presented. The results are discussed on the basis of the current density, I, for 0.89, 0.57 and 0.22 (A/cm^2) so that the behavior and response of the fuel cell can be studied under different load conditions.

4.1 Velocity and Pressure Fields

The inlet of the domain is chosen as the pressure inlet because the flow field has been developed for the interdigitated flow field design. For the velocity profile it can be seen that velocity is higher in the gas diffusion layer than in the catalyst layer. The velocity difference in the two layers can be attributed to: 1) due to the selection of flow field design; as both inlet and outlet are on the same side, the flow tends to follow the shortest path and 2) permeability of gas diffusion layer is higher than the catalyst layer. The flow field as obtained is shown in Figure 8, while, the pressure field for the simulated domain is given in Figure 9. The values given in the figure represent the pressure difference between the display location and the outlet. The overall pressure difference between the inlet and outlet is 550 N/m^2, where the outlet is at atmospheric pressure. It can also be noticed that the pressure drop is almost linear between the inlet and the outlet.
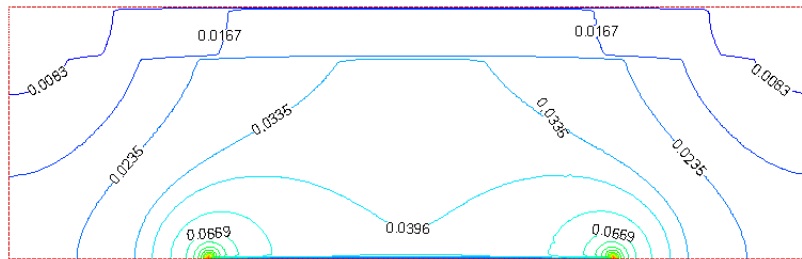

Figure 8: Velocity profile in the cathode of PEM fuel cell (m/s)

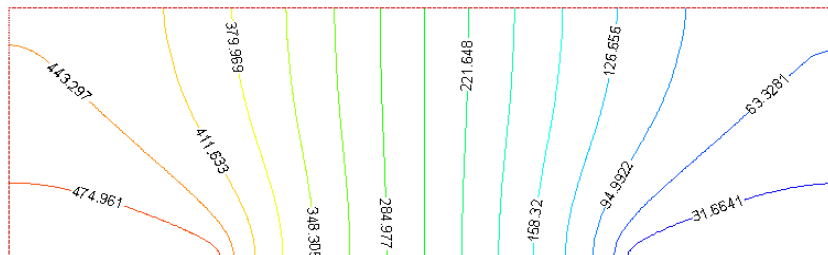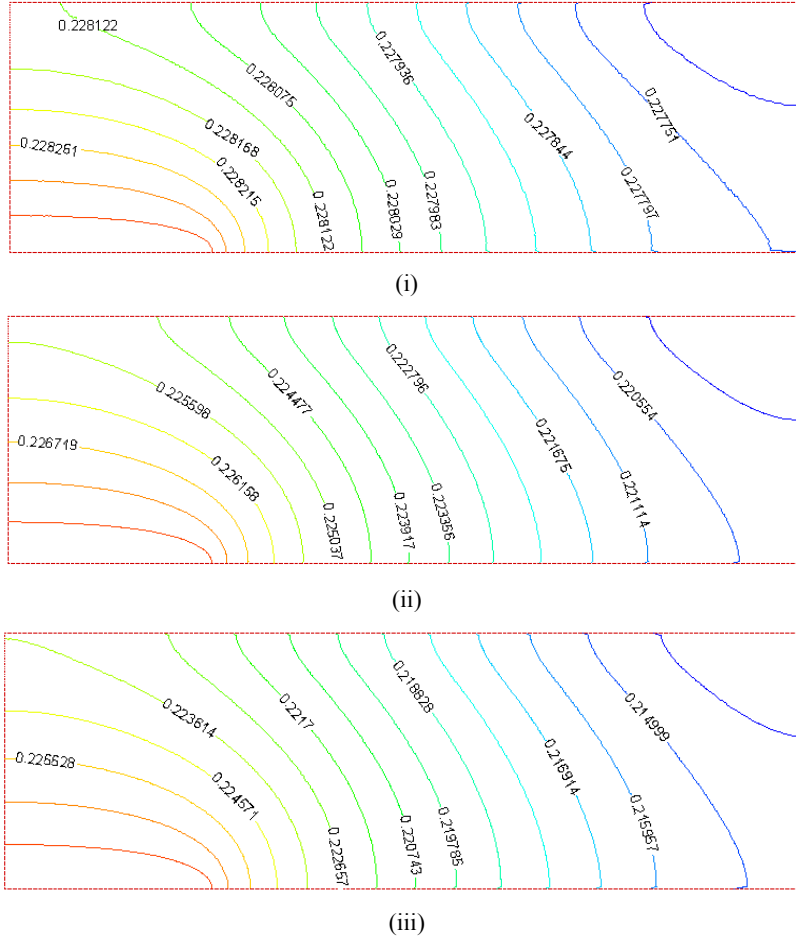**Figure 9: Pressure drop along the length of the cathode (N/m^2)**

(i)

(ii)

(iii)

Figure 10: Oxygen mass fraction at different current densities; (i) 0.22 (ii) 0.57 (iii) 0.89 A/cm^2

4.2 Oxygen Consumption

In PEM fuel cells, as already discussed, oxygen is used as the oxidant and is fed at the cathode inlet. The oxygen mass fraction is specified at the inlet of the domain. As the oxygen transverses the cathode, the electro-chemical reactions occur at the catalyst layer consuming oxygen.

Figure 10 represents the mass fraction of oxygen for different current density values. It can been seen that as the current density is increased, the consumption of oxygen also increases which can be correlated to the oxygen consumption rate. The oxygen mass fraction is lowest for current density of 0.89 A/cm^2 as compared to other values and small oxygen mass fraction is found close to the outlet in Figure 10 (iii) as compared to Figure 10 (i) and (ii).

4.3 Liquid Water Fraction

Due to the low operating temperatures, PEM fuel cells fall into the two-phase flow domain. The different sources for the liquid water considered here are;

1.   Electro – osmotic diffusion from membrane – source
2.   Back diffusion – sink
3.   Condensation – source
4.   Evaporation – sink

Water is an essential component for operation of PEM fuel cells because membrane hydration determines the membrane phase current (also called protonic current). Electro-osmotic diffusion of water is proportional to the current density i.e., at higher current density, there is higher protonic migration from anode to cathode, thus increasing the liquid water content. But, this increase in liquid water content, at very high current densities can result in clogging of the porous media generally referred as water flooding or water saturation and can cause severe mass limitations. Figure 11 represents the different water saturation levels for different levels of operation.
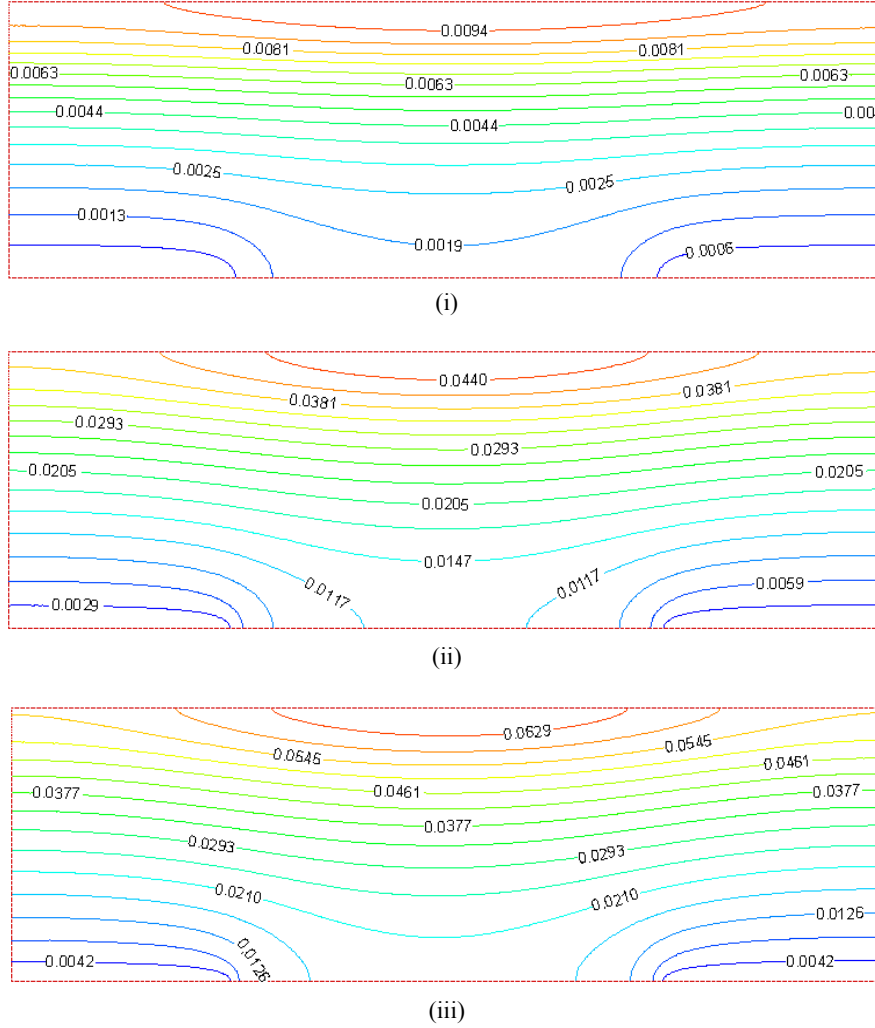

(i)

(ii)

(iii)

Figure 11: Volume fraction of liquid water at different current densities; (i) 0.22 (ii) 0.57 (iii) 0.89 A/cm^2
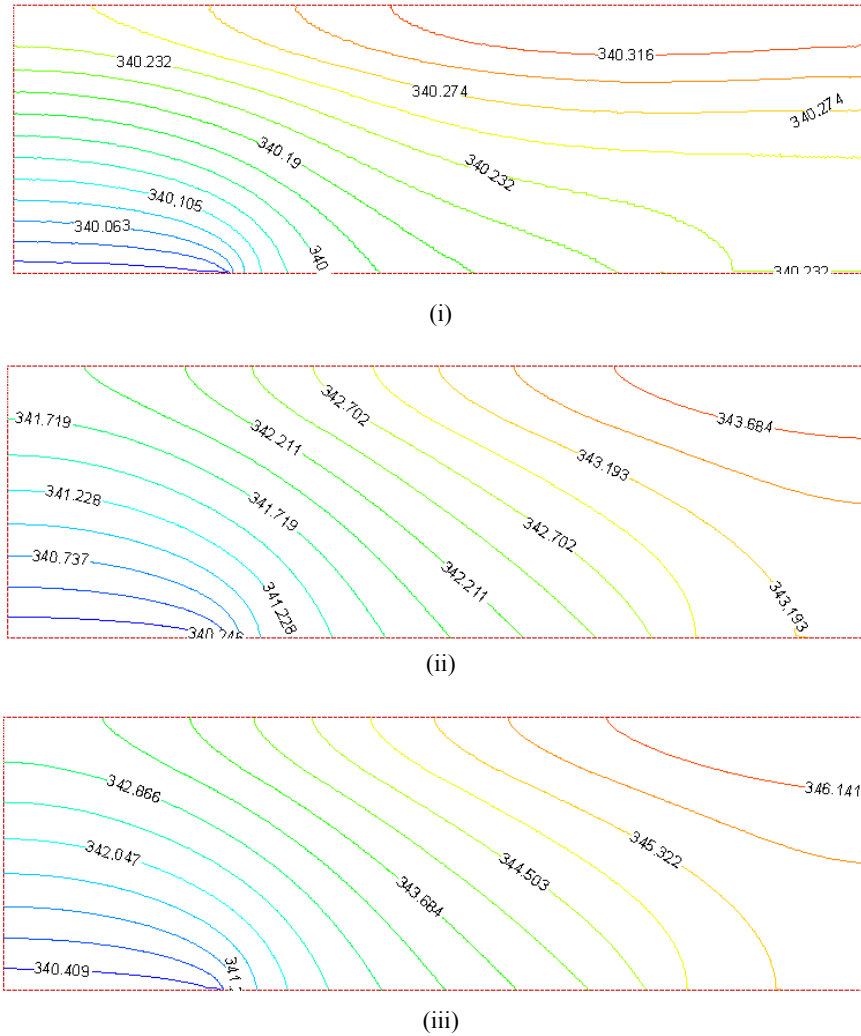
4.4   Temperature Distribution

The temperature increase in the cathode can be attributed to heat generated by electrochemical reactions and ohmic losses due to solid and membrane phase currents. Both ohmic losses and reaction rates are dependant on the current density. At higher current densities there is considerable increase in both the reaction rates and ohmic losses increase due to higher magnitude of current flows. Various sources for heat are explicitly given in Table 3: Source terms in two phase models.

Figure 12 shows the temperature distribution at the cathode for various current densities. The rise in the temperature at lower current densities is much smaller as it is being balanced by the

evaporation/condensation rates but as we approach higher current density levels, due to considerable increase in reaction rate and current flow, the temperature rise is much higher.

In the gas diffusion layer there is inter transfer of heat to care the non-thermal equilibrium effects. At the cathode inlet, the fluid temperature is at inlet conditions i.e. 340 K. So, at inlet, heat is transferred from solid phase to fluid phase or solid matrix is being cooled by the fresh air. In the catalyst layer, both fluid phase and solid phase are fixed at same temperature utilizing the fact that the reactions occur at the fluid/solid interface. But, near the outlet region of the cathode, fluid phase is at higher temperature, so, heat is transferred from fluid to solid phase thus causing a decrease in the temperature. The temperature distribution in the solid phase is represented in Figure 13.

In previous works, when only single phase fluid model was considered, it was observed that the temperature rise predicted were higher as compared to two phase flow. The difference in the results can be explained as; for two phase flows, in a unit control volume, the temperature change is being also balanced by phase change (Appendix 'A' and 'B').
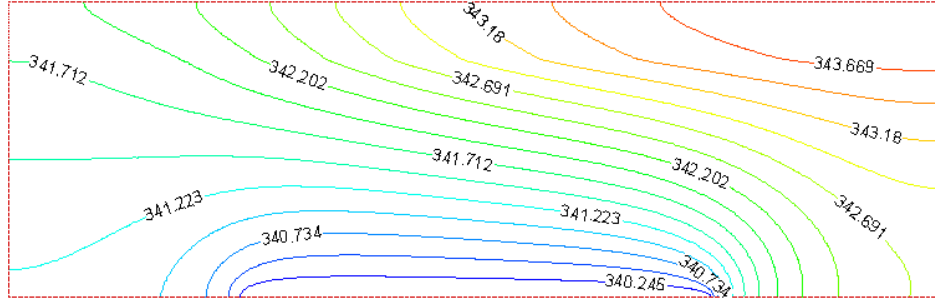

(i)

(ii)

(iii)

Figure 12: Fluid Temperature (K) distribution in cathode for various current densities; (i) 0.22 (ii) 0.57 (iii) 0.89 A/cm^2
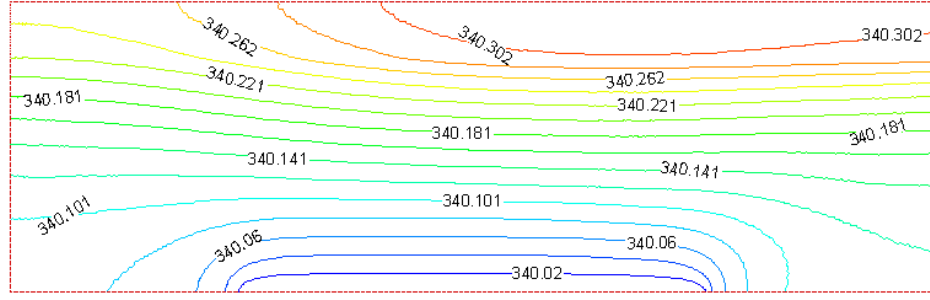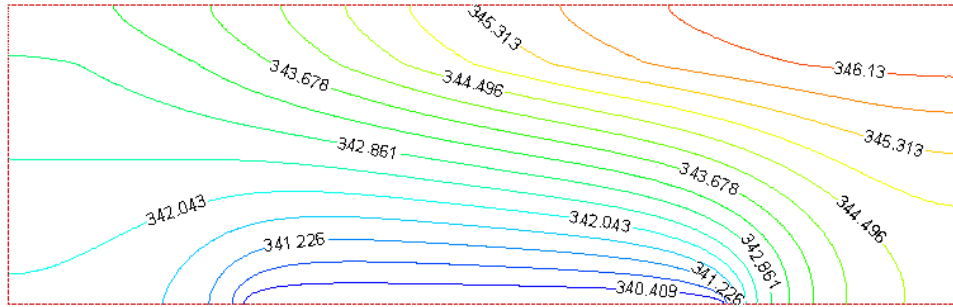
(i)

(ii)

(iii)

Figure 13: Solid phase Temperature (K) distribution for various current densities; (i) 0.22 (ii) 0.57 (iii) 0.89 A/cm^2

4.5   Membrane and Solid Phase Potentials

Since the interface at the membrane/catalyst has been used as the boundary condition for defining the nominal cathode overpotential, the local distribution of membrane phase potential is according to the value of NCO. But, the membrane phase conductivity, as given in Equation (38), is highly dependant on the water activity. It can be seen in Figure 14 (i) that at lower current densities, due to less osmotic drag and water production, the membrane phase conductivity decreases along the length of the cathode. The inlet humidification is very essential at low current densities to keep it humid all the times when internal production is quite less. But, as the current density increases, the water production rate increases and the osmotic drag is also increased, therefore, the solid phase conductivity at different location follows the rising pattern, see Figure 14 (ii). But the increase in the conductivity at higher current density has to be balanced by the inlet humidification, otherwise clogging will occur.
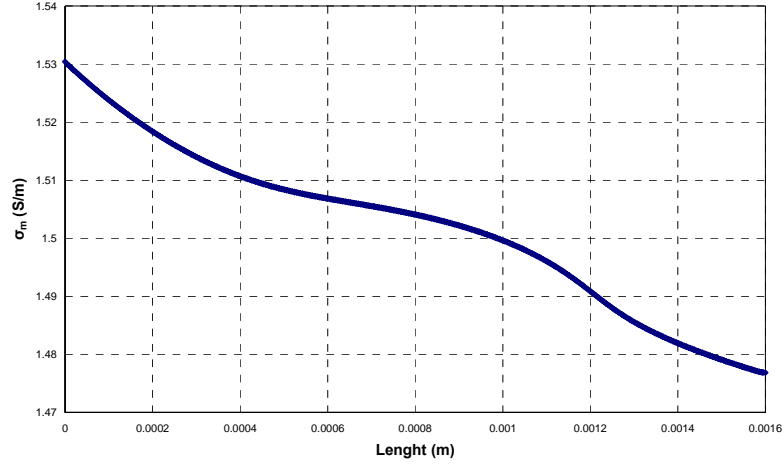
(i)
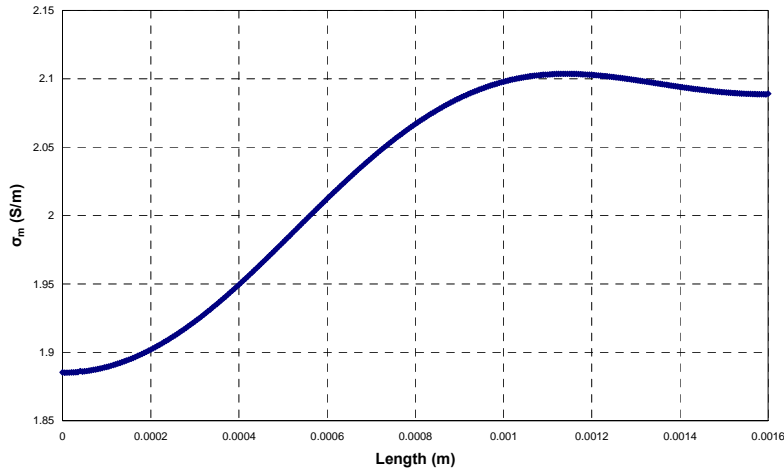
(ii)

Figure 14: Membrane Phase conductivity at y = 0.4 and 0.5 mm for current densities of 0.22 and 0.89 A/cm^2

The local solid phase potential variation is shown in Figure 15. The local potential is higher at the corners of the catalyst layer. The variation in the local solid phase potential can be attributed to the solid phase conductivity which is a function of both porosity and the fraction of electrolyte present. In the present case the electrolyte fraction of 0.5 has been assumed.
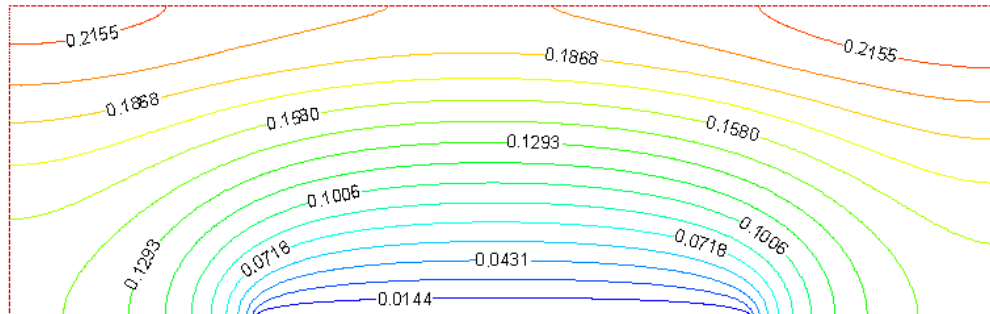
Figure 15: Local solid phase potential distribution for the cathode

Figure 16 represents the difference in the nominal cathode overpotential that is applied as boundary condition and the local cathode overpotential at membrane/catalyst interface. It can be seen that at lower currents, the difference is small showing less wastage of energy in driving the electro-chemical reactions.

38

While, at higher current densities, due to increased reactions, a considerable amount of energy is wasted in driving the reactions.
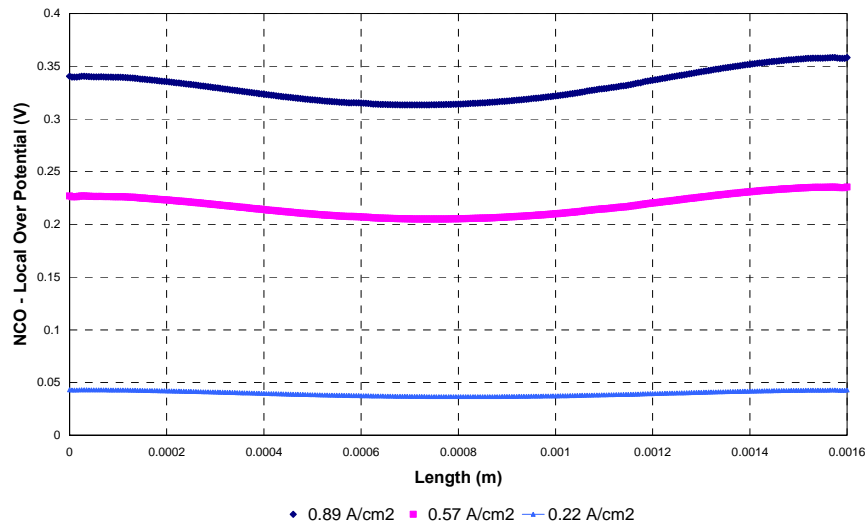

Figure 16: Local cathode potential for various load conditions (y = 0.5 mm)

4.6   Model Verification and Comparison

The verification of fuel cell models is usually carried out using the polarization curve by comparing it to experimental data. In present scenario, due to lack of the experimental data, this model has been compared to the earlier model presented by Sun et al. [18]. The model presented by Sun et al. included the agglomerate modeling approach for the catalyst layer but involves only gas phase i.e., liquid water effect has been neglected. It can be seen in Figure 17 that both the models are in good agreement at lower current densities. But, as the current density is increased, the model of Sun et al. over predicts the current because it does not include the water flooding effect that causes the reduction in porosity and active sites for chemical reactions. Also, the present model has been compared to the earlier work and a considerable difference is seen in the predicted values of current densities.
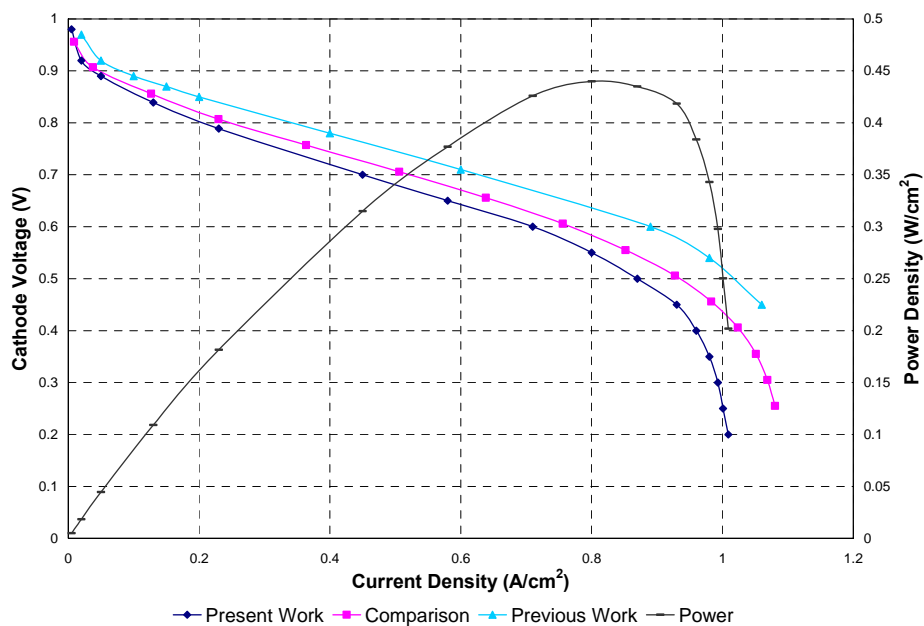

Figure 17: Polarization curve comparison and power density curve

5   Conclusions

In this work, the CFD approach has been implemented to the cathode of a PEM fuel cell to study different parameters under varying load conditions. The modeling approach was based on two phase flow (liquid and gas), two phase current (solid and membrane) and two phase temperature (fluid and solid) to get a better understanding of the fuel cell performance and various phenomena.

It was observed that the presence of liquid water affects the overall performance of the cell. At lower current densities, there is less production of water (less electro-chemical reactions and less electro-osmotic drag), the inlet humidity plays a vital role in keeping the cell upto required humidity level. But as the current density is increased, there is more production of water due to increased reaction rate and electro-osmotic drag. This increase in water production can cause severe water flooding and reduce the performance of the fuel cell. It is also observed that the temperature rise at low current densities is quite low as compared to temperatures at higher current densities. For fluid phase temperatures, in all cases, a rising pattern was observed along the length of the cathode. Since, the solid phase and fluid phase temperature is assumed to be the same in the catalyst layer, it essentially follows the same rise as the fluid phase temperature, but, in the gas diffusion layer, near the inlet of the cathode, the solid phase temperature is higher than the incoming fluid phase temperature. This difference in the temperatures near the inlet, causes cooling of the solid phase. While, near the outlet of the cathode, the fluid phase temperature is higher than the solid phase temperature, causing a net flow of heat to the solid phase. Since the conduction of solid phase is much higher than the fluid phase conduction, the temperature rise is limited to much lower values by conducting the heat to the current collector which is maintained at 340 K (assumption).

The solid phase conductivity that is modeled as a function of solid phase porosity and the membrane fraction present in the solid matrix, remains almost constant throughout the simulation domain. But the membrane phase conductivity, which is a function of water activity, shows a varied behavior under different conditions. At lower currents, there is a decreasing pattern observed along the length of the cathode showing a significant dehydration effect because of less water production inside cathode. But, at higher current densities and higher water activity, the membrane phase conductivity also showes an increasing behavior. These different responses of the membrane phase conductivity show the strong dependence of PEM fuel cells on water activity.

It was also observed that the losses are much more at higher current densities due to driving more reactions for increased current and the increased heating effects due to flow of charges. By comparing the nominal cathode overpotential and local overpotential, it was also observed that the difference in two was much more for higher currents as more energy was wasted in driving the electro-chemical reactions.

By utilizing the agglomerate catalyst layer modeling approach, the mass limitation effects are seen at higher current density due to lack of oxidant transport to the reaction sites to balance the increased reaction rates and this effect is further enhanced due to the presence of liquid water by covering the reaction sites.

Overall, as it can be seen in the comparison with other models, the current model is much more conservative in approach and effectively displays the interconnection of all phenomena in the PEM fuel cells. The maximum power density for the PEM fuel cells was obtained at approximately at 0.55 V which is lower than the single phase flows.

Since, only the cathode side is simulated in this study, the effects of anode e.g. heat losses due to charge flow, are neglected, it is suggested that the same modeling approach should be applied for a complete cell and the total response should be studied for thorough understanding the effects of anodic reactions coupled with the cathode to get an overall picture that will be very helpful in increasing the confidence level for PEM fuel cells as an alternate source for clean, cheap and reliable energy.

6.   References

1.   Jacobson D (2004) PEM fuel cell basics: physics.nist.gov/MajResFac/NIF/pemFuelCells.html.

2.   Basu S (2007) Recent trends in fuel cell science and technology Asamaya Publishers, New Delhi

3.   Larminie J, Dicks A (2003) Fuel Cell Systems Explained, 2nd edn John Wiley & Sons Ltd., West Sussex

4.   Das SK, Bansode AS (2009) Heat and mass transport in proton exchange membrane fuel cells - A review. Heat Transfer Engineering 30: 691-719

5.   Prater K (1990) The renaissance of solid polymer fuel cell. J Power Sources 29: 239-250

6.   Bernardi DM (1990) Water-balance calculations for solid-polymer-electrolyte fuel cells. J Electrochem Soc 137: 3344-3350

7.   Okada T, Xie G, Tanaba Y (1996) Theory of water management at the anode side of polymer electrolyte of polymer electrolyte fuel cell membranes. J Electroanalytical Chem 413: 49-65

8.   Yi JS, Nguyen TV (1999) Multicomponent transport in porous electrodes of proton exchange membrane fuel cells using interdigitated gas distributors. J electrochem Soc 146: 38-45

9.   Wang ZH, Wang CY, Chen KS (2001) Two-phase flow and transport in the air cathode of proton exchange membrane fuel cells. J Power Sources 94: 40-50

10.   Weber AZ, Newman J (2006) Coupled thermal and water management in polymer electrolyte fuel cells. J electrochem Soc 153: 2205-2214

11.   Nguyen TV, White RE (1993) A water and heat management model for proton-exchange membrane fuel cells. J electrochem Soc 140: 2178-2187

12.   Yuan J, Sundén B (2004) Numerical analysis of heat transfer and gas flow in PEM fuel cells. Numerical Heat Transfer (Part A) 38: 111-128

13.   Yuan J, Sundén B, Hou M, Huamin Z (2004) Three-dimensional analysis of two-phase flow and its effects on the cell performance of PEMFC. In: Francis T (ed) Numerical Heat Transfer: Part A, pp. 669-694.

14.   Garau V, Barbir F, Liu H (2000) An analytical solution of a half-cell model for PEM fuel cells. J electrochem Soc 147: 2468-2477

15.   Um S, Wang CY, Chen KS (2000) Computational fluid dynamics modeling of proton exchange membrane fuel cells. J electrochem Soc 147: 4485-4493

16.   Hwang AJJ, Chao CH, Chang CL, Ho WY, Wang DY (2007) Modeling of two-phase temperature in a two-layer porous cathode of polymer electrolyte fuel cells. Intl J Hydrogen Energy 32: 405-414

17.   Hwang JJ, P.Y. C (2006) Heat/mass transfer in porous electrodes of fuel cells. Intl J Heat and Mass Transfer 49: 2315-2327

18.   Sun W, Peppley BA, Karan K (2005) An improved two-dimensional agglomerate cathode model to study the influence of catalyst layer structural parameters. Electrochem Acta 50: 3359-3374

19.   Sun W, Peppley BA, Karan K (2005) Modeling the influence of GDL and flow-field plate parameters on the reaction distribution in the PEMFC cathode catalyst layer. J Power Sources 144: 42-53

20.   Hwang AJJ (2007) A complete two-phase model of a porous cathode of a PEM fuel cell. J Power Sources 164: 174-181

21.   Chang S-M, Chu H-S (2007) A transient model of PEM fuel cells based on a spherical thin film-agglomerate approach. J Power Sources 172: 790-798

22.   Senn SM, Poulikakos D (2005) Multiphase transport phenomena in the diffusion zone of a PEM fuel cell. J Heat Transfer 127: 1245-1259

23.   He W, Yi JS, Nguyen TV (2000) Two-phase flow of the cathode of PEM fuel cells using interdigitated flow fields. AIChE Journal 46: 2053-2064

24.   He G, Yamazaki Y, Abdula A (2009) A droplet size dependent multiphase mixture model for two phase flow in PEMFCs. J Power Sources 194: 190-198

25.   Berning T, Lu DM, Djilali N (2002) Three dimensional computational analysis of transport phenomena in PEM fuel cells. J Power Sources 106: 284-294

26.   Harvey D, Pharoah JG, Karan K (2008) A comparison of different approached to modeling the PEMFC catalyst layer. J Power Sources 179: 209-219

27.   Merk HJ (1958) The macroscopic equations for simultaneous heat and mass transfer in isotropic, continuous and closed systems. Appl Sci Res 8: 73-99

28.   (2009) User's guideAnsys Fluent 12.

29.   Yuan J, Lv X, Sundén B, Yue D (2007) Analysis of parameter effects on the transport phenomena in conjunction with chemical reactoins in ducts relevant for methane reformers. Intl J Hydrogen Energy 32: 3887-3898

30.   Reid CR, Prausnitz JM, E. PB (1986) The properties of gases & liquids, 4th edn McGraw-Hill Book Company, New York

31.   Nam JH, Kaviany M (2003) Effective diffusivity and water-saturation distribution in single- and two-layer PEMFC diffusion medium. Int J Heat Mass Transfer 46: 4595-4611

32.   Nguyen TV (1999) Modeling two-phase flow in the porous electrodes of proton exchange membrane fuel cells using interdigitated flow fields. Tutorials in Electrochemical Engineering Mathematical Modeling 14: 222-241

33.   Moran MJ, Shapiro HN (1999) Fundamentals of engineering thermodynamics, 4th edn John Wiley & Sons, New York

34.   Dutta S, Shimpalee S, Van Zee JW (2001) Numerical prediction of mass-exchange between cathode and anode channels in a PEM fuel cell. Int J Heat Mass Transfer 44: 2029-2042

35.   Janssen GJM, Overvelde MLJ (2001) Water transport in the proton-exchange-membrane fuel cells: measurements of the effective drag coefficient. J Power Sources 101: 117-125

36.   You L, Liu H (2002) A two phase flow and transport model for cathode of PEM fuel cells. Int J Heat Mass Transfer 45: 2277-2287

37.   Choi KH, Peck DH, Kim CS, Shin TH, Lee TH (2000) Water transport in polymer membranes for PEMFC. J Power Sources 86: 197-201

38.   Chao CH, Hwang AJJ (2006) Predictions of phase temperatures in a porous cathode of polymer electrolyte fuel cells using a two-equation model. J Power Sources 160: 1122-1130

39.   Ju H, Meng H, Wang C-Y (2005) A single phase, non-isothermal model for PEM fuel cells. Intl J Heat and Mass Transfer 48: 1303-1315

40.   Gallart MS (2007) Computational modeling and optimization of proton exchange membrane fuel cellMecahanical Engineering University of Vectoria.

41.   (2009) Fuel cell module manualAnsys Fluent 120.

42.   Springer TE, Zawodzinski TA, Gottesfeld S (1991) Polymer electrolyte fuel cell model. J Electrochem Soc 138: 2334-2342

43.   Lipkowski J, Ross PN (1998) Electrocatalysis Wiley-VCH

44.   Siegel NP, Ellis MW, Nelson DJ, Spakovsky MRv (2003) Single domain PEMFC model based on agglomerate catalyst geometry. J Power Sources 115: 81-89

Appendix A

SPECIES AND TEMPERATURE DISTRIBUTION IN CATHODE OF PEMFC

Munir A. Khan, Jinliang Yuan and Bengt Sundén

Department of Energy Sciences, Faculty of Engineering
Lund University, Box 118, SE-221 00 Lund, Sweden

ABSTRACT

In this work, the cathode side of proton exchange membrane fuel cells (PEMFCs) in contact with an interdigitated gas distributor has been numerically simulated using a commercial software for the species transport and temperature distribution of the fluid and solid phases. It has been found that the maximum temperature in the fluid phase occurs at the stagnation zones where the fluid is almost stationary. The local thermal equilibrium (LTE) model was incorporated in the catalyst layer while the local thermal non-equilibrium (LTNE) approach was utilized in the diffusion layer where inter-transfer of energy takes place due to the temperature difference in the fluid and solid phases. It is observed that the temperature distribution of the fluid phase was dependent on the value of interstitial heat transfer coefficient. The fluid phase temperature approaches the solid phase temperature distribution at higher values of interstitial heat transfer coefficient.

INTRODUCTION

In search for an alternative energy sources, the proton exchange membrane fuel cells (PEMFCs) have emerged as one of the most appreciated competitors. But in order to compete on commercial scale, still many phenomena need to be understood and in-depth research has to be carried out to fully understand the behavior of PEMFCs under different situations and environment. Among others, species transport and temperature distribution inside the cell are the major parameters affecting the performance and behavior. Also, other parameters like physical structure, inlet conditions, pressure, and flow field distribution also need to be associated with temperature and species transport because of the coupling among each other. Hence, in PEMFCs, a mathematical model is needed which incorporates all the factors and simultaneously represents the contribution of all performance parameters on the actual operation of a fuel cell.

With the availability of high speed computing and commercial and in-house CFD softwares, different modeling techniques and methodologies for PEMFCs have emerged. As far as the catalyst layer is concerned, initially, it was modeled as a thin interface layer and all the reactions were assumed to occur in that layer [1,2,3]. Another model used for the catalyst layer is the discrete-volume model [4,5,6,7]. The discrete-volume model has been able to produce more realistic results as compared to the thin interface model but couldn't provide insight of catalyst layer physical structure and its limitations.

In addition to the above models for the catalyst layer, the agglomerate model is considered the most detailed one of all as it incorporates the physical structure of the catalyst layer while in the other models the reactions are considered to occur uniformly in the volume of the catalyst layer [8,9,10]. One of the first agglomerate catalyst layer model was presented by [11] where it was shown that the catalyst layer is made up of clumps of carbon supported platinum catalyst surrounded by thin a layer of electrolyte and showed that the agglomerate catalyst layer model has been able to produce more detailed behavior compared to other models. A detailed study was also performed by [10] to physically support the agglomerate model in which different imaging techniques were used to validate the agglomerate catalyst layer model. In the present study the agglomerate model has been incorporated for the simulation.

As for the temperature field, the LTNE approach has been utilized in the diffusion layer while in the catalyst layer where both the solid and fluid phases are assumed to be in thermal equilibrium because of the chemical reactions occurring at the interface of solid and fluid phases, so, the temperature difference between solid and fluid phase is much smaller than the overall temperature difference between inlet and outlet of the domain [12]. But in gas diffusion layer, the temperature difference between the solid and fluid phase is dependent on the value of the interstitial

heat transfer coefficient, so, the 2-equation model (LTNE) is incorporated for simulating the temperature in the diffusion layer [13,14,15].

NUMERICAL MODEL

Figure and Table 1 show the layout and dimensions of the cathode side of the PEMFC in contact with the interdigitated flow field. In the present model, only the cathode side is considered due to its slow kinetics as compared to the anode side reactions. On the cathode side, the oxygen reduction reaction (ORR) is given as;

$$O_2 + 4e^- + 4H^+ \rightarrow 2H_2O \qquad (1)$$
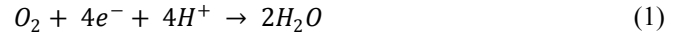
The mixture of oxygen and water vapors enter the domain from the inlet and transverses through the domain towards the outlet. The chemical reactions occur in the catalyst layer of the module and as the mixture transverses through the module, oxygen is consumed and water vapor is produced. Also, due to the chemical reactions occurring in the catalyst layer, heat is also generated which is either convected to the outlet or conducted through the solid matrix of the catalyst and diffusion layers to the current collector (called rib hereafter).

Assumptions

1. The fuel cell is operating at steady conditions.
2. Inlet mixture is modeled as ideal, laminar, incompressible.
3. All thermal properties of both mixture and module materials are considered constant.
4. The gas diffusion layer is composed of void spaces and carbon fibers.
5. The catalyst layer is composed of agglomerates made of platinum particles supported on carbon and ionomer electrolyte.
6. The inlet and rib temperature is uniform.
7. Water exits as gas only.
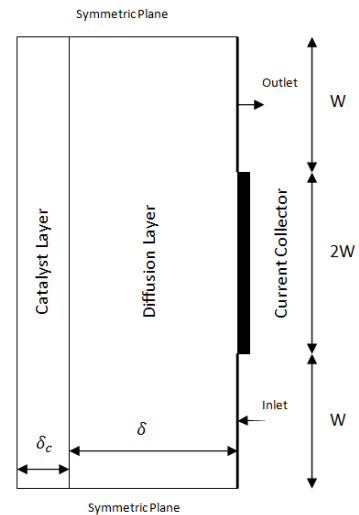

Figure 1: Layout of cathode side domain of a PEMFC connected with interdigitated flow field

Table 1: Geometric dimensions of cathode side domain

Geometric Parameters	Dimensions
Module Length	$L = 160\ \mu m$

Catalyst layer thickness	$\delta_c = 10 \ \mu m$
Diffusion layer thickness	$\delta = 40 \ \mu m$
Channel width	$2W = 80 \ \mu m$
Shoulder Width	$Ws = 80 \ \mu m$

Governing Equations

In both catalyst and diffusion layers of the module, the steady volume-average continuity and momentum equation are solved, given as [9,13,14,16];

$$\nabla(\rho \boldsymbol{u}_{Darcy}) = S_1 \tag{2}$$

whereas ;

$$\boldsymbol{u}_{Darcy} = \varepsilon(\boldsymbol{u}_{Physical}) \tag{3}$$

and,

$$S_1 = -S_{O_2,RXN} + S_{H_2O,RXN} + S_{H_2O,flux} \tag{4}$$

The source term S_1 in Eq. (2) consists of water vapor production due to the chemical reactions in the catalyst layer and water vapor flux from the membrane and sink for oxygen also due to the chemical reactions. For the diffusion layer, the source term S_1 is zero.

$$\rho_f \boldsymbol{u} \cdot \nabla \boldsymbol{u} = -\nabla p + \nabla \cdot (\mu \nabla \boldsymbol{u}) + S_2 \tag{5}$$

Eq. (5) is the momentum equation where S_2 consists of two sources, $S_{2,1}$ and $S_{2,2}$. First source term $S_{2,1}$ consists of two parts: a viscous and an inertial loss terms [16], given as:

$$S_{2,1} = \left(\sum_{j=1}^{2} D_{ij} \mu \boldsymbol{u}_j + \sum_{j=1}^{2} C_{ij} \frac{1}{2} \rho |\boldsymbol{u}| \boldsymbol{u}_j \right) \tag{6}$$

In present model, the inertial loss term is neglected and homogeneous porous media conditions are applied, the Eq. (6) reduces to;

$$S_{2,1} = -(\mu D \boldsymbol{u}) \tag{7}$$

The other source in the momentum equation Eq. (5) consists of terms due to subtraction of oxygen and addition of water vapor due to chemical reactions and flux, which is accounted by [9];

$$S_{2,2} = S_1 \boldsymbol{u} \tag{8}$$

Species Distribution

The mixture in the module is considered to consist of two species, i.e., oxygen and water vapor, both in the same phase. The governing equation for the species distribution is given as [9,13,14,16];

$$\nabla \cdot (\rho \boldsymbol{u} Y_i) = -\nabla \cdot \boldsymbol{J}_i + S_3 \tag{9}$$

The source term S_3 in Eq. (9) accounts for one sink term for oxygen which is being consumed and two source terms for water vapor due to chemical reactions and back diffusion. Also, in Eq. (9) $\boldsymbol{J}_i$ is the diffusion flux of species i which arises due to concentration gradient given by [16];

$$\boldsymbol{J}_i = -\rho D_{i,eff} \nabla Y_i \tag{10}$$

The effective diffusion coefficient for species i follows the Bruggmann model [17] i.e.,

$$D_{i,eff} = \varepsilon^{1.5} D_i \tag{11}$$

Temperature Distribution

The temperatures in both the solid and fluid phases in the catalyst and diffusion layers are modeled by applying the energy equation.

Catalyst Layer

Since the chemical reactions only take place in the catalyst layer, so the energy equation contains a source term for heat, given as [13,14];

$$(\rho c_P)_f \boldsymbol{u} \cdot \nabla T_f = \nabla \cdot (k_{C,eff} \nabla T_f) + S_4 \tag{12}$$

The source term in Eq. (12) represents the overpotential heating by the chemical reactions taking place in the catalyst layer. In the catalyst layer, the LTE approach has been incorporated so the inter-transfer of energy between solid and fluid phases is zero, i.e., both the phases are assumed to be at the same temperature. The effective thermal conductivity for the catalyst layer can be determined by the following equation [13,18];

$$k_{C,eff} = -2k_C + \frac{1}{\frac{\varepsilon_C}{2k_C + k_f} + \frac{1 - \varepsilon_C}{3k_C}} \tag{13}$$

Diffusion Layer

In the diffusion layer, the LTNE approach has been utilized [14]. The equations for the solid and fluid phases are given as [13,14,19];

$$(\rho c_P)_f \boldsymbol{u} \cdot \nabla T_f = \nabla \cdot (k_{f,eff} \nabla T_f) + S_5 \tag{14}$$

$$0 = \nabla \cdot \left(k_{S,eff} \nabla T_f \right) + S_6 \tag{15}$$

Whereas, the source terms S_5 and S_6 in Eqs. (14) and (15) describe the inter transfer of energy due to the temperature difference of the two phases given as [13,14];

$$S = h_V \left(T_S - T_f \right) \tag{16}$$

Along with the convective heat transfer between the phases, joule heating source is also included for the solid phase due to flow of charges. The effective thermal conductivities of the fluid and solid phases are given as [13,14];

$$k_{f,eff} = \varepsilon k_f \tag{17}$$
and,
$$k_{s,eff} = (1 - \varepsilon) k_s \tag{18}$$

Modeling Source terms based on the agglomerate model

All the governing equations, as described in the previous sections remain the same for all type of catalyst layer models except for the source terms that are utilized to account for different species transport and reaction mechanism. In the agglomerate model, oxygen travels to the surface of the agglomerate and dissolves into the electrolyte phase. Once oxygen has been dissolved into the electrolyte, it is transported through the electrolyte film which has engulfed the agglomerate.

In order to describe the agglomerate catalyst model, standard Butler-Volmer kinetics can be utilized as [20];

$$i = a_{Pt}^{eff} i_0 \frac{C_{O_2}}{C_{O_2}^{reff}} \left[\exp\left(-\frac{\alpha_C F}{RT} \eta_{act} \right) - \exp\left(\frac{(1 - \alpha_C)F}{RT} \eta_{act} \right) \right] \tag{19}$$

W. Sun *et. al* [8] has provided the governing kinetics equation after detailed re-arrangement, and has been used in the present model.

$$i = 4F \frac{p_{tot} Y_{O_2}}{H_{O_2-N}} \left(\frac{1}{E_r k_c (1 - \varepsilon_C)} + \frac{(r_{agg} + \delta_{agg})\delta_{agg}}{a_{agg} r_{agg} D_{O_2,N}} \right)^{-1} \tag{20}$$

where E_r is the effectiveness factor and is given by [9];

$$E_r = \frac{1}{\emptyset_L} \left(\frac{1}{\tanh(3\emptyset_L)} - \frac{1}{3\emptyset_L} \right) \tag{21}$$

Thiele's modulus for a spherical agglomerate, $\emptyset_L$, is given by [9];

$$\emptyset_L = \frac{r_{agg}}{3} \sqrt{\frac{k_c}{D_{eff}}} \tag{22}$$

The reaction rate constant k_c, is [14];

$$k_c = \left(\frac{a_{Pt}^{agg}}{zF(1 - \varepsilon_c)} \right) \left(\frac{i_o}{C_{O_2}^{reff}} \right) \left[\exp\left(-\frac{\alpha_c F}{RT} \eta_{act} \right) - \exp\left(-\frac{(1 - \alpha_c)F}{RT} \eta_{act} \right) \right] \tag{23}$$

On the basis above discussed agglomerate catalyst model, the source terms for different governing equations are summarized in Table 2.

Table 2: Source terms based on the agglomerate catalyst model for governing equations.

$S_{O_2,RXN}$	$\frac{M_{O_2}}{4F} i$
$S_{H_2O,RXN}$	$\frac{M_{H_2O}}{2F} i$
$S_{H_2O,flux}$	$\frac{2\alpha M_{H_2O}}{2F} i$
S_4	$i\eta$

The source term for the water flux accounts for electro-osmotic drag and back diffusion. The convection of the water vapors from membrane towards cathode due to the pressure gradient that arises due to capillary pressure and elastic stresses have been ignored in the current model.

Table 3: Operating conditions

Inlet temperature	333K
Rib temperature	333K
Inlet O_2 concentration	0.98%
Inlet H_2O concentration	0.019%

Table 4: Properties of cathode used in current model

Thermo-Physical Properties	Density (solid)	1100 kg.m^{-3}	[13]
	Density (fluid)	1.13 kg.m^{-3}	[13]
	Thermal conductivity (solid)	1.71 Wm^{-2}K^{-1}	[13]
	Thermal conductivity (fluid)	0.051 Wm^{-2}K^{-1}	[21]
	Viscosity	1.5863x10^{-5} m^{2}s^{-1}	[13]
	Interstitial heat transfer coefficient	10^3-10^8 W.m^{-3}.K^{-2}	
	Stiochiometric flow ratio	5.0	[13]
Geometric Properties	GDL Porosity	48%	[13]
	CL Porosity	42%	[13]
	CL Viscous Resistance	9.775x10^{11} m^{-2}	[13]
	GDL Viscous Resistance	6.537x10^{11} m^{-2}	[13]
	Surface to volume ratio	1000 m^{-1}	[13]
Agglomerate Properties	Platinum loading	4 g.m^{-3}	[9]
	Platinum radius	1.5 nm	[9]
	Agglomerate radius	1 μm	[9]
	Effective agglomerate area	3.6x10^5 m^{2}m^{-3}	[9]
	Reference exchange current density	3.85x10^{-4} A.cm^{-2}	[9]
	Activation energy	76.5x10^3 J.mol^{-1}	[9]
	Charge transfer	1	[9]
	Reference O_2 Concentration	3.6551 mol.m^{-3}	[21]
	Henry's Constant	2685x10^8 Pa.m^3.mol^{-1}	[9]
	Effective Pt surface ratio	0.75	[9]

NUMERICAL METHODS

All the governing equations were numerically solved using third order of discretization with residual convergence limited to 10-6 for all variables. The grid independency was achieved at 200×500 (x×y) after which the change in maximum temperature was less than 0.1%.

RESULTS AND DISCUSSION

Flow Field

As can be seen in Figure 2, the magnitude of flow velocity is much higher in the gas diffusion layer than in the catalyst layer which can be attributed to higher porosity and permeability of the gas diffusion layer. Also, since the path followed by the fluid has to be least resistive, the velocity magnitude near the rib at inlet and outlet are much higher. The weakest flow velocity occurs at the top left and bottom left corners.

Species Distribution

Figure 3 and 4 represent the species distribution under the operating conditions given in Table 2. Initially the concentration of O_2 is higher but as the mixture transverses and diffuses upwards, due to the chemical reaction occurring in the catalyst layer, the concentration of O_2 decreases. On the contrary, the concentration of H_2O is initially less but increases as the mixture approaches the domain outlet. To calculate the diffusivity of the mixture, the constant dilute-approximation method has been incorporated in the present model.
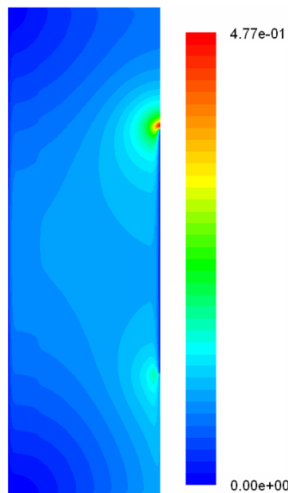

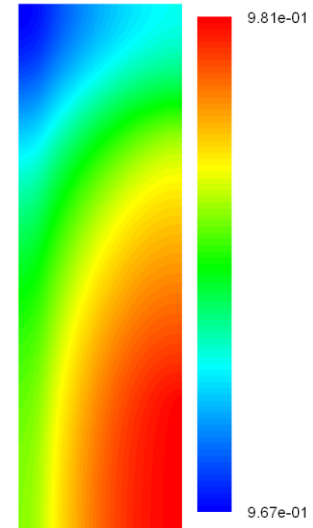**Figure 2: Flow field distribution inside cathode of polymer electrolyte fuel cell**
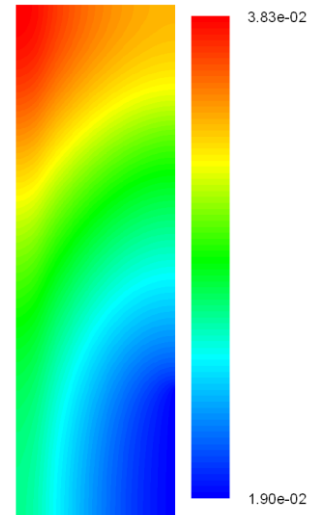

Figure 3: O_2 concentration distribution

Figure 4: H_2O concentration distribution

It was also observed that by increasing the inlet temperature, the consumption of O_2 showed a decreasing pattern which can attributed to the fact that the activation losses are higher at higher temperatures due to increase in the exchange current density [22].

Temperature Distribution

The temperature distribution for the current simulation has been carried out for different interstitial heat transfer coefficients. For small values of the interstitial heat transfer coefficient (1×10^3 $Wm^{-3}K^{-1}$), both solid and fluid phases have high temperature in the catalyst layer because of the chemical reactions. But in the increasing x-axis direction, the fluid and solid phases start to differ from each other because of low inter convective heat transfer in the gas diffusion layer. At the module inlet, the fluid phase has lower temperature because of the fresh mixture coming in and cools the solid phase due to convection as shown in

Figure 5. As the fluid is convected towards the module outlet, the temperature of the fluid increases but near the module outlet, the temperature of the fluid phase is higher than the solid phase (Figure 6) because of the heat added due to the chemical reactions. Hence, at the module outlet the heat is convected to solid phase and results in elevated temperature of the solid phase.
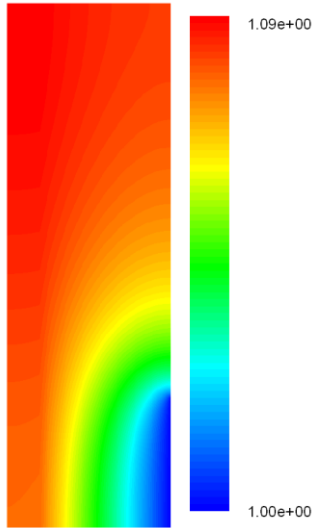

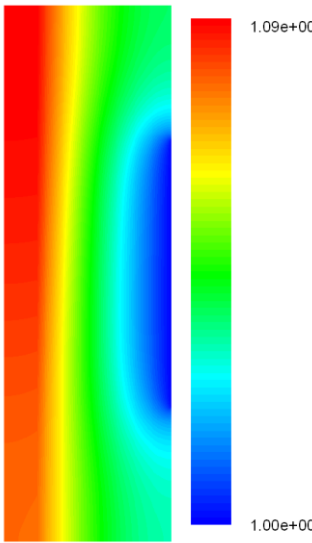**Figure 5: Fluid phase temperature distribution of cathode (T/T$_{in}$, h$_v$=1x10^3)**

Figure 6: Solid phase temperature distribution of cathode (T/T$_{in}$, h$_v$=1x10^3)

For high values of the interstitial heat transfer coefficient (1x10^8 Wm^{-3}K^{-1}), the temperature distribution is almost the same for both phases because of the high convective heat transfer between the phases (Figure. 7,8). Also, the solid phase has higher thermal conductivity than the fluid phase and the maximum temperature level is also reduced. Hence, for preventing high local hot spots, along with the thermal conductivities of both fluid and solid phases, the interstitial heat transfer coefficient plays an important role.

CONCLUSION

Species concentration and two-phase temperatures of PEMFC are solved numerically using commercial CFD software. The catalyst layer is simulated using the agglomerate catalyst model and the LTNE approach is utilized in thermal analysis of solid and fluid phase temperatures.
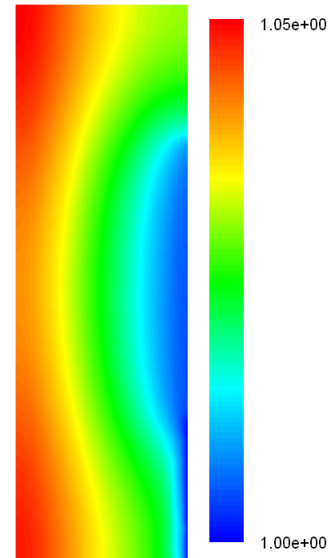
Figure 7: Fluid phase temperature distribution of cathode (T/T$_{in}$, h$_v$=1x10^8)
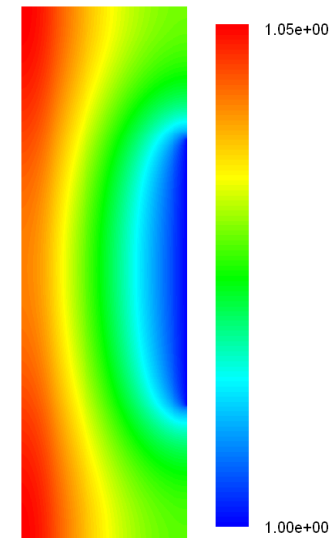
Figure 8: Solid phase temperature distribution of cathode (T/T$_{in}$, h$_v$=1x10^8)

Results show that the consumption rate along with physical parameters of the agglomerate geometry is also dependent on operating conditions and environment. The temperature was found highest in the catalyst layer, which is obvious due to the chemical reactions taking place there while within catalyst layer it was higher in the upper and

lower left corners of the domain due to stagnation zones with maximum value occurring at the upper left corner. In the stagnation zone, conduction through the solid phase overwhelmes the convection heat transfer. Due to the LTNE approach, the inter transfer of energy was also observed in the gas diffusion layer with fluid temperature distribution approximately approaching the solid phase distribution as the value of interstitial heat transfer coefficient was big $(1 \times 10^8 \text{ Wm}^{-3}\text{K}^{-1})$.

ACKNOWLEDGMENTS

REFERENCES

[1] T. Berning, N. Djilali, "A 3D, Multi-Phase, Multicomponent Model of the Cathode and Anode of a PEM Fuel Cell", J. Electrochem Soc. 150(12)(2003): A1589-A1598.

[2] P.W. Li, L. Schaefer, Q.M. Wang, T. Zhang, M.K. Chyu, "Multi-gas Transport and Electrochemical Performance in a Polymer Electrolyte Fuel Cell with Complex Flow Channels," J. Power Sources 115(2003): 90-100.

[3] B.R. Siversten, N. Djilali, "CFD Based Modelling of Proton Exchange Membrane Fuel Cells", J. Power Sources 141(2005) 65-78.

[4] M. Bang, M. Odgaard, T.J. Condra, S.K. Kaer, Proceedings of 2nd International Conference on Fuel Cell Science, Engineering and Technology, 2004.

[5] M. Bang, S. Yde-Anderson, T.J. Condra, N. Djilali, E. Skou, Proceedings of the conference on Hydrogen and Fuel Cells, 2003.

[6] S. Um, C.Y. Wang, "Three-dimensional Analysis of Transport and Electrochemical Reaction in Polymer Electrolyte Fuel Cells" J. Power Sources 125(2004): 40-51.

[7] T. Zhou, H. Liu, "A 3D Model for PEM Fuel Cells Operated on Reformate", J. Power Sources 125(2004): 101-110.

[8] Sun, W., B.A. Pepply, K. Karan. "An improved two-dimensional agglomerate cathode model to study the influence of catalyst layer structural parameters." Electrochem. Acta 50(16-17)(2005): 3359-3374.

[9] D. Harvey, J.G. Pharoah, K. Karan. "A comparison of different approaches to modeling the PEMFC catalyst layer." J. Power Sources 179(2008): 209-219.

[10] N.P. Siegel, M. W. Ellis, D. J. Nelsen, M. R. von Spakovsky. "Single domain PEMFC model based on agglomerate catalyst geometry." J. Power Sources 115(2003): 81-89.

[11] K. Broka, P. Ekdunge. "Modeling the PEM fuel cell cathode." J. Appl. Electrochem 27(1997): 281-289.

[12] M. Kaviany, Principles of heat transfer in porous media. 2nd ed. Springer, 1995.

[13] J.J. Hwang. "Heat transfer in porous electrode of fuel cells." J. Heat Transfer, 128(2006): 434-443.

[14] J.J. Hwang, P.Y. Chen. "Heat/mass transfer in porous electrodes of fuel cells." Int. J. Heat and Mass Transfer 49(2006): 2315-2327.

[15] C.H. Chao, Azai J.J. Hwang. "Prediction of phase temperatures in porous cathode of polymer electrolyte fuel cells using two-equation model", J. Power Sources, 160(2006):1122-1130.

[16] Fluent User's Guide, Fluent Inc. 2006.

[17] H. Oldham, J. Myland, "Fundamentals of electrochemical science." Acedemic Press, New York, 1994.

[18] J.J. Hwang, C.K. Chen, D.Y. Lai. "Detailed characteristic comparison between planar and MOLB-type SOFCs." J. Power Sources 143(2005): 75-83.

[19] C.H. Chao, C.L. Chang, W.Y. Ho, D.Y. Wang, "Modeling of two phase temperature in a two-layer porous cathode of polymer electrolyte fuel cells", Int. J. Hydrogen Energy, 32(2007): 405-414.

[20] A.J. Bard, L.R. Faulkner, Electrochemical methods-Fundamentals and Application, 2nd ed. John Wiley and Sons Inc. New York, 2001.

[21] J.J. Hwang, "A complete two-phase model of a porous cathode of a PEM fuel cell", J. Power Sources, 164(2007): 174-181.

[22] J. Larminie, A. Dicks, "Fuel Cell Systems Explained", "2nd ed., John Wiley and Sons, 2003.

Appendix B

LTNE approach to simulate temperature of cathode in a PEMFC

Munir Ahmed Khan, Jinliang Yuan, Bengt Sundén

Munir.khan@energy.lth.se, Jinlian.Yuan@energy.lth.se, Bengt.Sunden@energy.lth.se

Department of Energy Sciences, Faculty of Engineering

Lund University, Box 118, SE-221 00 Lund, Sweden

Ph: +46-46-2228604, Fax:+46-46-2224717

Abstract

The solid phase and fluid phase temperature and species distribution have been calculated numerically in this study. The model considered here consists of catalyst layer, porous-transport layer and the current collector region (rib). Two energy equations approach has been employed in the porous transport layer and one energy equation is solved for the catalyst layer to simulate the temperature distribution. Full multi-component diffusion model and Knudsen effect have been included for the simulation of the species distribution in both catalyst and porous-transport layer. The agglomerate model has been used to simulate the catalyst layer. It has been found that the diffusion coefficient is low in the catalyst layer due to low permeability and porosity causing stagnation zones and the temperature rise is maximum in the stagnation zones causing local hot spots.

Keywords: Numerical study; Two equation energy approach; Agglomerate Model; Diffusion Coefficient; Stagnation Zones

1. Introduction

Polymer electrolyte membrane fuel cells (PEMFCs) have attained a considerable amount of attention in the research society in the last decade for their habit as environment friendly and high efficiency energy production units for both mobile and stationary units. Only few hurdles need to be overcome before PEMFCs can be launched in full commercial scale. One of the major hurdles still faced by the PEMFCs is their water management. PEMFCs use a solid polymer like SOFCs which give these two a major advantage over other fuel cell counterparts because of their stability. But, in PEMFCs, the ionic conductivity of the electrolyte is strongly dependant on the water content; more water content means higher conductivity. So, it is imperative for electrolyte to be damped at all times. On the

other hand, high water content in the cell can choke the flow of oxidant to the reaction site causing shutting down of the system. In order for the PEMFCs to work, a good water balance has to be maintained in the cell [1]. In conjunction to the above stated balance, thermal distribution in the cell plays a vital role in balancing the water content while the inlet supply is pre-humidified.

Since practical measurements are difficult to perform inside the fuel cell due to its compact nature and in order to visualize the internal behavior and response of the cell to the operating conditions, numerical simulations are mostly relied upon and in order to achieve reliable and accurate results, catalyst layer has been the main focus of interest because of the electro-chemical reactions occurring in it [2]. Up till now, many different approaches have been applied to simulate the catalyst layer where the agglomerate model has produced more explanatory results of the actual behavior of a PEMFC [2-5].

In this study, the transport phenomenon has been studied in depth for simulating the temperature distribution in the cathode side of a low pressure operating PEMFC. Since PEMFCs are low temperature operating devices, i.e., the temperature difference between the inlet and outlet is very low, thus a low temperature difference between the solid and fluid phase cause significant local thermal non-equilibrium (LTNE) [6]. Then separate energy equations are employed for the solid and fluid phases with inter transfer of energy among them.

2. Numerical models and equations

A schematic drawing of a typical porous cathode in contact with an interdigitated flow field of a PEMFC is given in Figure 1. The present computation is limited to a repeated section between the inlet and outlet channel.

The air-water vapor mixture enters into the porous cathode from the section inlet and transverses the porous transport layer (PTL) to the catalyst layer. The oxygen reduction reaction occurring in the catalyst layer consumes oxygen and, meanwhile produces water vapor. It can be presented as;

$$O_2 + 4H^+ + 4e^- \longleftrightarrow 2H_2O \qquad\qquad (1)$$

During the reaction, heat due to overpotential and irreversibility is generated. It should be removed from the cathode by the fluids or the solid.

Model Assumptions

The following assumptions have been made in the present model;

1. The cell is operating at steady conditions.

2. Inlet mixture is modeled as ideal and laminar flow.

3. The PTL is composed of void spaces and carbon fibers.

4. The catalyst layer is composed of agglomerate made of platinum particles supported by carbon and ionomer electrolyte.

5. The inlet and current collector temperature is uniform.

6. Water exits as gas only.

Governing Equations

In both catalyst and porous transport layers, the steady volume averaged continuity and momentum equations are solved, i.e.,

$$\nabla(\rho \cdot u_{Darcy}) = S_1 \qquad (2)$$

and,

$$\rho_f u \cdot \nabla u = -\nabla p + \nabla \cdot (\mu \nabla u) + S_2 \qquad (3)$$

The source term in (2) denotes the increase and decrease in the mass flow rate of the species due to chemical reactions occruing in the catalyst layer and back flow and osmotic drag of water to and from the membrane. The source term in (3) accounts for the viscous loss term as given in Table 1.

The species transport in the present study is handled by the general transport equation given by

$$\nabla \cdot (\rho u X_A) = -\nabla \cdot J_A + S_3 \qquad (4)$$

where J_A is the diffusion flux for a species i and is given by

$$J_A = -\rho D_{A,eff} \nabla X_A \qquad (5)$$

The diffusion coefficient $D_{A,gm}$ of a particular species in (5) can be calculated based on the binary diffusion coefficients in the multi-component gas mixture [7, 8].

$$D_{A,gm} = \frac{1 - Y_A}{Y_B / D_{AB} + Y_C / D_{AC} + \cdots} \qquad (6)$$

Since the catalyst layer and the PTL are both porous media, Knudsen diffusion is an active phenomenon in the porous media and needs to be also accounted in the model [9].

$$D_{i,k} = \frac{2}{3} r_e v_i = \frac{2}{3} r_e \sqrt{\left(\frac{8RT}{\pi M_i}\right)} \qquad (8)$$

In the present model an effective diffusion coefficient has been estimated based on both molecular and Knudsen diffusion given as [7];

$$D_{i,eff} = \varepsilon^\tau \left(\frac{D_{i,gm} \times D_{i,k}}{D_{i,gm} + D_{i,k}}\right) \qquad (9)$$

The temperatures in both the solid and fluid phases in the catalyst layer and PTL are modeled by applying the energy equation. The effective thermal conductivity of both phases is calculated as [5, 6, 8, 10];

$$k_{f,eff} = \varepsilon k_f \tag{10}$$

and,

$$k_{s,eff} = (1 - \varepsilon)k_s \tag{11}$$

Since the chemical reactions are taking place in the catalyst layer, so the energy equation in the catalyst layer employs a source term for heat generation.

$$(\rho c_P)u \cdot \nabla T_f = \nabla \cdot (k_{f,eff} \nabla T_f) + S_4 \tag{12}$$

For the solid media, the energy equation is given as;

$$0 = \nabla \cdot (k_{s,eff} \nabla T_f) + S_5 \tag{13}$$

In the PEMFCs, the electrochemical reactions occur at the interface of the platinum catalyst surface and the fluid. Hence both the phases in the catalyst layer are assumed to be at the same temperature [6, 11, 12] i.e.;

$$T_f = T_s \tag{14}$$

Because two energy equations are solved for the porous transport layer, there is an inter-transfer of energy between the two phases as given in Table 1. The value of the interstitial heat transfer coefficient for the present case has been selected as 1.0×10^6 W·m^{-3}·K^{-1} [6].

Source Terms

All the governing equations, as described in the previous sections, remain the same for all type of catalyst layer models except for the source terms that are utilized to account for different species transport and reaction mechanism. In the agglomerate model, oxygen travels to the surface of the agglomerate and dissolves into the electrolyte phase. Once oxygen has been dissolved into the electrolyte, it is transported through the electrolyte film which has engulfed the agglomerate.

In order to describe the agglomerate catalyst model, standard Butler-Volmer kinetics can be utilized as [13];

$$i = a_{Pt}^{eff} i_o \frac{C_{O_2}}{C_{O_2}^{reff}} \left[\exp\left(-\frac{a_c F}{RT} \eta_{act} \right) - \exp\left(\frac{(1-a_c)F}{RT} \eta_{act} \right) \right] \tag{15}$$

For numerical simulations applications, the above equation can be arranged as [4, 5];

$$\nabla \cdot i = 4F \frac{P_{tot} X_{O_2}}{H_{O_2-N}} \left(\frac{1}{E_r k_c (1 - \varepsilon_c)} + \frac{(r_{agg} + \delta_{agg})\delta_{agg}}{a_{agg} r_{agg} D_{O_2,N}} \right)^{-1} \tag{16}$$

where H_{O_2-N} is Henry's constant which represents the solubility of oxygen into Nafion, and it can be estimated as [1];

$$H_{O_2-N} = 1.33 \times 10^{-6} \exp\left(\frac{-498}{T} \right) \times p \tag{17}$$

E_r is the effectiveness factor and for the spherical agglomerate as used in the present model, it is given by [4, 5];

$$E_r = \frac{1}{\Phi_L} \left(\frac{1}{\tanh(3\Phi_L)} - \frac{1}{3\Phi_L} \right) \tag{18}$$

Thiele's modulus for a spherical agglomerate, ϕ_L, and estimated by [4, 5];

$$\Phi_L = \frac{r_{agg}}{3} \sqrt{\frac{k_c}{D_{eff}}} \tag{19}$$

D_{eff} represents the diffusion of oxygen into Nafion and can be correlated using [1];

$$D_{eff} = \left(0.0031 \times 10^{-4} \left(-\frac{2768}{T} \right) \right) \times \phi_{agg}^{1.5} \tag{20}$$

The reaction rate constant k_c, is [4, 5, 14] ;

$$k_c = \left(\frac{a_{Pt}^{agg}}{zF(1-\varepsilon_c)} \right) \left(\frac{i_o}{C_{O_2}^{reff}} \right) \left[\exp\left(-\frac{a_c F}{RT} \eta_{act} \right) - \exp\left(-\frac{(1-a_c)F}{RT} \eta_{act} \right) \right] \tag{21}$$

The exchange current density i_0 is obtained by temperature corrected relation given as

$$i_0 = i_0^{ref} \exp\left[-\frac{E_{act}}{R} \left(\frac{1}{T} - \frac{1}{T_0} \right) \right] \tag{22}$$

On the basis of the above discussed agglomerate catalyst model, the source terms for different governing equations are summarized in Table 1. Table 2 gives the values for the model and kinetic parameters used in the current simulation.

The source term for the water flux accounts for electro-osmotic drag and back diffusion. The convection of the water vapors from membrane towards cathode due to the pressure gradient that arises due to capillary pressure and elastic stresses have been ignored in the current model.

3. Numerical Methods

For the present case, due to high inter dependency of species and temperature distribution along the domain, all the governing equations have been coupled and solved using 3rd order discretization with convergence criteria set to 10^{-6}. Grid independence was achieved at 220×514 uniform control volumes due to the simple case geometry. The inlet of the domain is treated as a pressure inlet while the interface between the catalyst layer and membrane is set as an adiabatic wall by assuming that there is no transfer of energy over this interface. The inlet temperature of the fluid phase and the temperature of the current collector have been fixed at a steady value of 340K.

4. Results and Discussion

The velocity distribution for the cathode side is shown in Figure 2. Velocity is minimal in the catalyst layer due to lower permeability of the catalyst layer. Within the PTL, the velocity is comparatively higher in the region near the current collector because of the shorter flow path. Stagnation zones are created in the upper and lower left corners of the domain causing temperature rise being maximum as heat conduction remains the only mode of heat transfer.

In the cathode side, pre-humidified air (O_2, H_2O and N_2) with mass fractions of 0.2284, 0.0198 and 0.7518 enters into the domain and transverses through both the porous transport and catalyst layers. In the catalyst layer oxidation reduction reactions occur as given in Eq. (1). The reaction rate is dependant on quite many parameters including both physical and operating parameters. The physical parameters are accounted for by using the agglomerate model.

Initially the oxygen concentration is high, hence the chemical reaction rate is large but as the mixture transverses the domains the reaction rate decreases and becomes small due to consumption of oxygen. Since, in the catalyst layer, the reaction rate is highly dependent on the presence of oxygen in the domain, so in the present study a multi-component diffusion model is used for in-depth distribution analysis including the Knudsen diffusion. For density and specific heat capacity calculations, the volume-weighted mixing law has been incorporated. The numerical result of the species distribution is shown in Figure 3.

Figure 4 shows the temperature distribution inside the cathode of a PEMFC. In the catalyst layer, since the electro-chemical reactions are assumed to occur at the interface of the solid and fluid phase, the fluid and solid phases are considered to have same temperature [6, 11, 12]. In PTL, a two-equation model has been incorporated by employing separate energy equations for the solid and fluid phases with inter transfer of energy. The temperature of the solid phase in PTL is lower than the fluid phase because the solid has higher thermal conductivity. At the inlet, the fluid enters the domain with a uniform temperature and is heated up due to transfer of energy from the solid phase, whereas, the solid phase is cooled by the fresh inlet fluid. Near the exit of the domain, the fluid phase is at higher temperature than the solid phase due to the chemical reactions occurring in the catalyst layer. The solid phase is then heated up by the fluid phase.

5. Conclusion

In the present study, the cathode side of a low pressure PEMFC has been simulated using an agglomerate and two equation thermal model at high operating voltage. For species distribution, a multi-component diffusion model has been incorporated where density and specific heat capacity has been calculated by volume-weighted mixing law. All the parameters are strongly temperature dependent while the reaction rate is coupled with the distribution of species within the domain. It has been observed that higher temperature leads to higher reaction rates but the oxidant concentration limits the rise due to the decrease in concentration as the mixture transverses towards the module outlet. The diffusion coefficient is minimum in the catalyst layer due to the low porosity and permeability.

Stagnation zones are created in the catalyst layer leading to which local hot spots where heat conduction is the primary cooling phenomenon.

5. Nomenclature

a_{agg}	Effective agglomerate surface area ($m^2 \cdot m^{-3}$)
a_{Pt}^{eff}	Effective catalyst surface area ($m^2 \cdot m^{-3}$)
a_c	Cathodic transfer coefficient
c_p	Specific heat capacity ($J \cdot kg^{-1} \cdot K^{-1}$)
$C_{O_2}^{ref}$	Reference O_2 concentration ($mol \cdot m^{-3}$)
$D_{i,eff}$	Effective diffusivity of species i ($m^2 \cdot s^{-1}$)
$D_{A,gm}$	Binary diffusion coefficient of species in mixture ($m^2 \cdot s^{-1}$)
D_{eff}	Effective diffusivity of dissolved oxygen in electrolyte ($m^2 \cdot s^{-1}$)
F	Faraday's constant
H	Henry's constant ($Pa \cdot m^3 \cdot mol^{-1}$)
h_v	Interstitial heat transfer coefficient ($W \cdot m^{-3} \cdot K^{-1}$)
k_c	Reaction rate constant (s^{-1})
i	Current density ($A \cdot m^{-2}$)
i_o	Local exchange current density ($A \cdot m^{-2}$)
M	Molecular weight of gas mixture ($kg \cdot mol^{-1}$)
M_i	Molecular weight of species ($kg \cdot mol^{-1}$)
m_{Pt}	Platinum loading ($kg \cdot m^{-2}$)
u	Velocity vector ($m \cdot s^{-1}$)
p	Pressure (Pascals)
r_{agg}	Radius of agglomerate (m)

R	Universal gas constant ($J\cdot mol^{-1}\cdot K^{-1}$)
X	Species mass fraction
Y	Species molar fraction
z	Number of electrons consumed per mole of reactant

Greek Letters

α	Net drag coefficient of water molecule per proton
δ_{agg}	Thickness of electrolyte film covering an agglomerate (m)
ε_{agg}	Proportion of electrolyte in agglomerate
ε	Porosity of material
ε_c	Porosity of catalyst layer
Φ_L	Theile's modulus
η_{act}	Local activation overpotential (V)
ρ	Density ($kg\cdot m^{-3}$)

Subscripts and superscripts

|	
agg	Agglomerate
c	Catalyst layer
eff	Effective
f	Fluid phase
i	Species
Pt	Platinum
s	Solid phase

7. References

1.   Chang, S.-M. and H.-S. Chu, *A transient model of PEM fuel cells based on a spherical thin film-agglomerate approach.* J. Power Sources, 2007. **172**: p. 790-798.

2.   Siegel, N.P., et al., *Single domain PEMFC model based on agglomerate catalyst geometry.* J. Power Sources, 2003. **115**(1): p. 81-89.

3.   Broka, K. and P. Ekdunge, *Modelling the PEM fuel cell cathode.* J. Appl. Electrochem, 1997. **27**: p. 281-89.

4.   Harvey, D., J.G. Pharoah, and K. Karan, *A comparison of different approaches to modeling the PEMFC catalyst layer.* J. Power Sources, 2008. **179**: p. 209-19.

5.   Sun, W., B.A. Peppley, and K. Karan, *An improved two-dimensional agglomerate cathode model to study the influence of catalyst layer structural parameters.* Electrochem. Acta, 2005. **50**(16-17): p. 3359-74.

6.   Hwang, J.J. and Chen. P.Y., *Heat/mass transfer in porous electrodes of fuel cells.* Intl. J. Heat and Mass Transfer, 2006. **49**: p. 2315-27.

7.   Haberman, B.A. and J.B. Young, *Three-dimensional simulation of chemically reacting gas flows in the porous support structure of an integrated-planar solid oxide fuel cell.* Intl. J. Heat and Mass Transfer, 2004. **47**: p. 3617-29.

8.   Yuan, Jinliang, XinRong Lv, Bengt Sunden, Dantin Yue , *Analysis of parameter effects on the transport phenomena in conjunction with chemical reactoins in ducts relevant for methane reformers.* Intl. J. Hydrogen Energy, 2007. **32**: p. 3887-98.

9.   Reid, C.R., J.M. Prausnitz, and P.B. E., *The properties of gases & liquids.* 4th ed. 1986, New York: McGraw-Hill Book Company.

10. *Fluent user's guide*: Fluent Inc.

11. Hwang, A.J.J., *A complete two-phase model of a porous cathode of a PEM fuel cell.* J. Power Sources, 2007. **164**: p. 174-81.

12. Hwang, A.J.J., et al., *Modeling of two-phase temperature in a two-layer porous cathode of polymer electrolyte fuel cells.* Intl. J. Hydrogen Energy, 2007. **32**: p. 405-14.

13. Bard, A.J. and F. L.R., *Electrochemical methods-Fundamentals and Applications.* 2nd ed. 2001, New York: John Wiley & Sons Inc.

14. Gallart, M.S., *Computational modeling and optimization of proton exchange membrane fuel cells*, in *Mechanical Engineering*. 2007, University of Victoria.
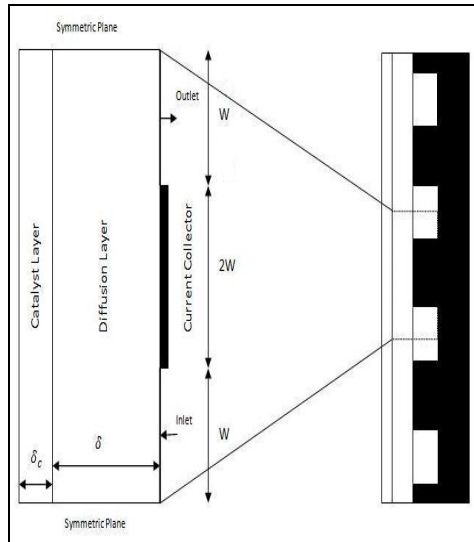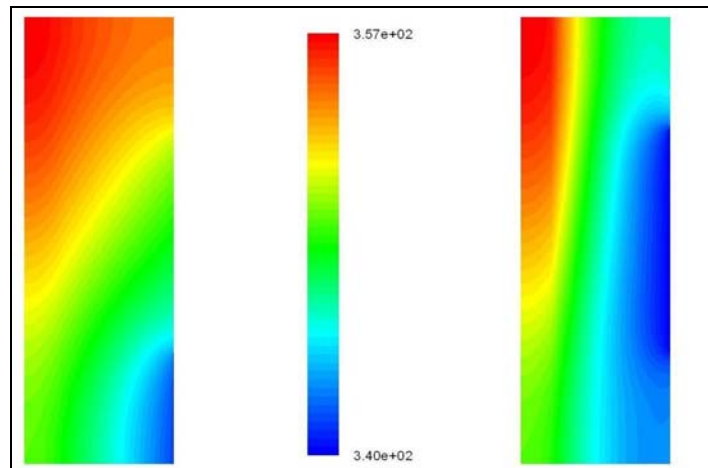
Figure 1: Schematic drawing of a porous electrode of the interdigitated flow field
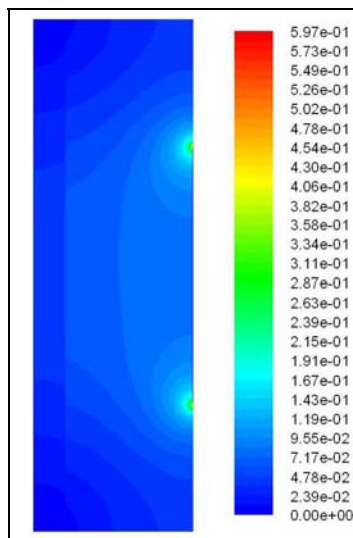
Figure 2: Velocity magnitude distribution pattern in cathode of PEMFC (m/s)
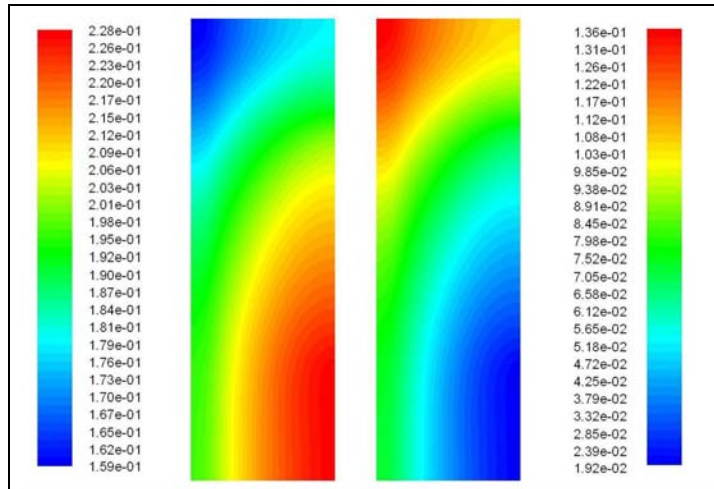
Figure 3: Mass fraction distribution in the cathode of PEMFC: (Left) O₂; (Right) H₂O

Figure 4: Temperature (K) distribution inside cathode of a PEMFC:(Left) Fluid Phase; (Right) Solid Phase

Table 1: Source terms based on agglomerate model

	Source terms	
	Catalyst Layer	Porous Transport Layer
Mass	$-\dfrac{M_{O_2}}{4F}\nabla\cdot i+\dfrac{M_{H_2O}}{2F}\nabla\cdot i+\dfrac{\alpha M_{H_2O}}{F}\nabla\cdot i$	0
Momentum	$S_{2,1}=-\left(\mu D_c u\right)$	$S_{2,1}=-\left(\mu D_{PTL}u\right)$
Species	$-\dfrac{M_{O_2}}{4F}\nabla\cdot i+\dfrac{M_{H_2O}}{2F}\nabla\cdot i+\dfrac{\alpha M_{H_2O}}{F}\nabla\cdot i$	0
Energy (Fluid)	$\eta(\nabla\cdot i)$	$h_v\left(T_s-T_f\right)$
Energy (Solid)	$T_s=T_f$	$-h_v\left(T_s-T_f\right)$

Table 2: Physical and kinetic parameters used in current model*

Thermo-Physical Properties	Density (solid)	1100 kg.m^{-3}
	Thermal conductivity (solid)	1.71 Wm^{-2}K^{-1}
	Thermal conductivity (fluid)	0.051 Wm^{-2}K^{-1}
	Viscosity	1.5863x10^{-5} m^{2}s^{-1}
	Interstitial heat transfer coefficient	10^6 W.m^{-3}.K^{-1}
	Stiochiometric flow ratio	5.0
Geometric Properties	GDL Porosity	48%
	CL Porosity	42%
	CL Viscous Resistance	9.775x10^{11} m^{-2}
	GDL Viscous Resistance	6.537x10^{11} m^{-2}

	Surface to volume ratio	$1000 \ m^{-1}$
Agglomerate Properties	Platinum loading	$4 \ g.m^{-3}$
	Platinum radius	1.5 nm
	Agglomerate radius	1 µm
	Effective agglomerate area	$3.6 \times 10^{5} \ m^{2}m^{-3}$
	Reference exchange current density	$3.85 \times 10^{-8} \ A.cm^{-2}$
	Activation energy	$76.5 \times 10^{3} \ J.mol^{-1}$
	Charge transfer coefficient	1
	Reference O_2 Concentration	$3.6551 \ mol.m^{-3}$
	Effective Pt surface ratio	0.75
	* [1, 3-5, 11, 14]	